Hyperactive neuronal networks enhance tau spread in an Alzheimer's disease mouse model

Aaron J. Barbour[1], Keegan Hoag[1], Eli J. Cornblath[1], Abigail Chavez[1], Alfredo Lucas[1], Xiaofan Li[1], Sydney Zebrowitz[1], Chloe Hassman[1], Omar Vazquez[2], Sharon X. Xie[2], Edward B. Lee[3, 4], Kathryn A. Davis[1], Virginia M.Y. Lee[4, 5, 6], Delia M. Talos[1*], Frances E. Jensen[1*]

[1]Department of Neurology, Perelman School of Medicine, University of Pennsylvania; Philadelphia, PA 19104, USA.

[2]Department of Biostatistics, Epidemiology, and Informatics, Perelman School of Medicine, University of Pennsylvania; Philadelphia, PA 19104, USA.

[3]Translational Neuropathology Research Laboratory, Perelman School of Medicine, University of Pennsylvania; Philadelphia, PA 19104, USA.

[4]Department of Pathology and Laboratory Medicine, Perelman School of Medicine, University of Pennsylvania; Philadelphia, PA 19104, USA.

[5]Institute on Aging, Perelman School of Medicine, University of Pennsylvania; Philadelphia, PA 19104, USA.

[6]Center for Neurodegenerative Disease Research, Perelman School of Medicine, University of Pennsylvania; Philadelphia, PA 19104, USA.

*Corresponding authors:

Frances E. Jensen, MD, FACP
Arthur Knight Asbury MD Professor
Chair, Department of Neurology
Hospital of the University of Pennsylvania, 3400 Spruce Street, Dulles 3
Philadelphia, PA 19104, PA USA
E-mail: frances.jensen@pennmedicine.upenn.edu

Delia Talos, MD
415 Curie Boulevard
263 Clinical Research Building
Philadelphia, PA, 19104
Phone: 215-573-8328, Fax: 215-662-3362
Email: talosd@pennmedicine.upenn.edu

Abstract

Pathological tau spreads via neuronal connections in Alzheimer's disease (AD). Given the high incidence and deleterious consequences of epileptiform activity in AD, we hypothesized that neuronal hyperactivity and seizures exacerbate tau spread. To examine the impacts of brain-wide network and population hyperactivity on tau spread, we created a novel mouse model involving the cross of targeted recombination in active populations (TRAP) and the 5 times familial AD mice (5X-TRAP) that allows for the permanent labelling of seizure-activated neurons. To explore the effects of seizures on tau spread, we injected these mice with human AD brain-derived tau to induce pathological tau spread, and induced seizures with pentylenetetrazol (PTZ) kindling. Brain mapping revealed that seizures increased tau spread in 5X-TRAP mice, which correlated extensively with memory deficits in PTZ kindled 5X-TRAP mice. Using computational models, we found data supportive of increased anterograde tau spread in 5X-TRAP mice and that regional neuronal activity levels were predictive of tau pathology. On a cellular level, we found that hyperactive neurons drive elevated tau propagation in 5X-TRAP mice. We also found corroborating evidence of increased tau spread in AD patients with a seizure history compared to those without. Our study identifies neuronal hyperactivity and seizures as key, targetable factors underlying AD progression.

63 # Introduction

64 The spread of the pathological tau protein is central to the progression of Alzheimer's disease
65 (AD), and proceeds along functional and neuroanatomical connections (1-6), with pathological
66 tau burden closely correlating with cognitive decline (7-10). Tau pathology in AD begins in the
67 locus coeruleus, and spreads to the entorhinal cortex, followed by the limbic system and
68 neocortex (10-12). In mice, intracerebral injection of human AD brain-derived tau lysate (AD-tau
69 seeding) results in misfolding and propagation of endogenous tau throughout the brain along
70 neuroanatomical connections (13), as seen in human AD. Tau spread is worsened by β–
71 amyloid (Aβ) pathology in humans (1, 14) and the five times familial AD (5XFAD) and other
72 amyloidogenic rodent models (15, 16). Studies have shown that neuronal activity can induce
73 synaptic tau release *in vitro* and can worsen local tau pathology *in vivo* (17), but direct evidence
74 that neuronal hyperactivity causes pathological tau spread throughout the brain *in vivo* is still
75 missing. A number of studies in mice and humans have demonstrated that the progressive
76 spread of tau pathology throughout the brain can be recapitulated in silico by computational
77 models of tau spread along structural connections between brain regions (18). Indeed, these
78 models provide quantitative evidence that tau spreads in both retrograde and anterograde
79 directions in seeded mice (19) and humans (1, 6, 20, 21). Understanding the factors that drive
80 both network and cellular level tau spread throughout the brain is poised to yield novel
81 therapeutic targets and strategies to slow disease progression.

82 Neuronal network hyperexcitability is prevalent in AD, particularly at early stages (22), with
83 unprovoked seizures occurring in up to 22% of AD patients (23). We and others have found
84 worsened AD pathology and cognitive outcomes in AD patients with a seizure history (23-28),
85 and AD-like pathology in temporal lobe epilepsy (29), suggestive of a bidirectional relationship
86 between network hyperactivity and AD. Similarly, neuronal hyperactivity is found in 5XFAD
87 mice, beginning at early, prodromal stages (24, 28) and Aβ-producing mouse models also show

88 neuronal hyperactivity at the cellular level (28, 30), with a positive feedback loop occurring
89 between neuronal hyperactivity and Aβ pathology (31, 32). Furthermore, seizure induction with
90 pentylenetetrazol (PTZ) kindling early in the disease progression worsens the progression of
91 amyloid pathology, excitatory: inhibitory imbalance, and cognitive deficits (24, 28, 33). While
92 network to cellular level neuronal hyperexcitability are well-characterized phenomena in AD, the
93 role of neuronal hyperactivity in the progression of tau spread is not well understood.

94 Recently developed genetic tools enable the permanent fluorescent (tdTomato, tdT) labeling
95 and tracking of transiently activated neuronal populations (Targeted Recombination in Active
96 Populations; TRAP), using the immediate early gene cFos as a proxy marker for neuronal
97 activity (34, 35). In murine epilepsy models, we and others have previously demonstrated that
98 neurons that underwent activity dependent tdT labelling during seizures have long-lasting
99 hyperexcitability, synaptic alterations, and demonstrate unique pathological effects (36-38) that
100 are promising therapeutic targets. However, the TRAP tool has not been used to date to
101 investigate hyperexcitability in neurodegeneration. Here, we created a novel model by crossing
102 TRAP mice with 5XFAD (5X-TRAP/WT-TRAP) to examine the interactions between tau spread
103 and neuronal hyperactivity on both a network and cellular level and track the contributions of
104 hyperactive populations to subsequent tau spread.

105 We hypothesized that neuronal hyperactivity in 5X-TRAP mice would be associated with
106 increased anterograde tau spread along neuronal networks and would be exacerbated by
107 seizure induction. To establish a causal role of seizures and neuronal hyperactivity in tau
108 propagation, we seeded WT-TRAP and 5X-TRAP mice with AD-tau in the right hippocampus
109 and overlying cortex to induce tau spread, induced seizures with PTZ kindling, and labelled
110 seizure-activated neurons with tdT. Using comprehensive brain mapping and computational
111 models of tau spread throughout neuroanatomical networks, we found that PTZ kindling in early
112 disease stages resulted in exacerbation of tau spread in 5X-TRAP mice through seizure-

activated circuits, and that network hyperactivity was associated with increased anterograde tau propagation. Memory deficits in PTZ kindled 5X-TRAP mice were highly correlated with tau spread and neuronal hyperactivity. Further, we found that hyperactive tdT+ neurons specifically drove increased tau spread in 5X-TRAP mice. To increase translational relevance, we examined the extent of tau pathology in human AD brain tissue and found evidence suggestive of increased tau spread in AD patients with a clinical seizure history compared to those without. Overall, these studies causally demonstrate that neuronal hyperactivity, via seizure induction, drives tau spread and suggest that hyperactive networks and neurons promote anterograde tau spread in AD. Thus, seizures and neuronal hyperexcitability are mitigatable and translatable targets to slow tau spread and AD progression.

Results

Novel 5X-TRAP mouse to study the interactions between AD pathology and neuronal activity

As our prior results revealed that seizure induction in 5XFAD mice early in the disease progression resulted in exacerbation of later memory deficits and brain pathology, we aimed to further study the interactions between neurodegeneration and neuronal activity at a population and network level. We thus developed a novel model by crossing hemizygous 5XFAD mice with mice homozygous for Fos$^{2A\text{-}iCreER}$ (TRAP2) and B6.Cg-*Gt(ROSA)26Sor*$^{tm14(CAG\text{-}tdTomato)Hze}$/J (Ai14) (Fig 1A). The resulting 5X-TRAP and WT-TRAP mice allow for robust, permanent tdT expression in neurons that express the activity-dependent cFos protein during a 4–6-hour window after 4-hydroxytamoxifen (4-OHT) induced CreER expression (Fig 1A). This novel 5X-TRAP model allows for the examination of the interactions between individual and brain-wide neuronal activity patterns and AD pathology.

136 5X-TRAP and WT-TRAP mice underwent unilateral AD-tau injection into the right hippocampus
137 and overlying cortex (posterior parietal association area) at 3 months of age, to initiate the
138 spread of pathological tau throughout the brain (13, 16) in mice that otherwise lack overt AT8
139 (phospho-tau Ser202/205) pathology (39). 2-3 weeks following AD-tau seeding, PTZ kindling or
140 control (saline, Sal) protocols were performed. On the final day of kindling (4 months of age),
141 mice were injected with 4-OHT to permanently label all basal or seizure activated neurons with
142 tdT. At 5-6 months of age, mice underwent behavioral testing and were euthanized at 6 months
143 of age (3 months post AD-tau injection) (Fig 1B). This model enabled the study of post-seeding
144 tau accumulation in basal and seizure activated networks, and in activated (tdT+) neurons to
145 determine whether these neurons were differentially affected from tdT- neurons.

146 We have previously demonstrated that PTZ induced seizures worsen Aβ pathology and memory
147 in the 5XFAD mouse (24). Here, we sought to establish whether seizures in WT-TRAP and 5X-
148 TRAP mice are responsible for worsening of tau spread throughout the brain, as tau is central to
149 cognitive decline and AD progression (7-10). We also examined brain-wide activity dependent
150 labeling (tdT) to determine whether 5X-TRAP mice display neuronal hyperactivity, and whether
151 early hyperactivity (tdT labeling at 4 months of age) is associated with subsequent tau spread.
152 Serially sectioned coronal samples spanning the majority of the brain from AD-tau seeded WT-
153 TRAP and 5X-TRAP mice were registered to the Allen Brain Atlas (ABA) and tau pathology,
154 assessed by AT8+ immunoreactive aggregates (AT8+ levels), along with detected tdT+ cells,
155 were mapped and quantified throughout the brain (Fig 1, S1, S2, S3, S4 and Tables S1, S2).

156 To assess the effects of PTZ treatment and 5XFAD genotype on brain-wide AT8+ levels and
157 tdT+ counts, linear mixed-effects statistical models were fit across all brain regions. We found a
158 significant increase in the estimated marginal means (EMM; a model adjusted means to control
159 for variations due to brain region and animal) in brain-wide AT8+ levels in Sal and PTZ treated
160 5X-TRAP compared to Sal and PTZ treated WT-TRAP mice and in PTZ treated 5X-TRAP

161 compared to Sal treated 5X-TRAP mice (Fig 1C), consistent with our hypothesis that seizures
162 drive tau spread in 5X-TRAP mice. With respect to activity dependent labeling, we found that
163 PTZ induced seizures increased EMM of brain-wide tdT+ counts in both genotypes compared to
164 Sal treated mice (Fig 1D), demonstrating increased activity-dependent neuronal labelling during
165 seizures, as we have previously observed (36). We also found increased brain-wide tdT+
166 counts in Sal treated 5X-TRAP mice compared to WT-TRAP, and in PTZ treated 5X-TRAP
167 compared to PTZ treated WT-TRAP (Fig 1D), demonstrating elevated basal and PTZ-induced
168 neuronal activity in 5X-TRAP mice.

169 To examine the effects of 5XFAD genotype and PTZ on tau spread and neuronal activity levels
170 in major brain structures, we used Bayesian statistics, as they provide full posterior distributions
171 of parameter estimates and are robust to relatively low sample sizes and hierarchical data
172 structures (40). Bayesian statistics identify credible effects, rather than p value-based
173 significance used in frequentist approaches (e.g. ANOVA). Models that accounted for region-
174 subregion relationships revealed credible interactions between 5XFAD genotype and PTZ
175 kindling to increase AT8+ levels in all 10 major brain structures examined (Fig S1). Credible
176 increases in tdT+ counts were also observed in all major brain structures examined due to PTZ
177 treatment, while interactions between 5XFAD genotype and PTZ treatment to increase tdT+
178 counts were limited to isocortex, olfactory areas, hippocampus, cortical subplate, and striatum
179 (Fig S2). Together, these models demonstrate substantial impacts of 5XFAD genotype and PTZ
180 kindling to increase tau spread and activity dependent labeling in all major brain structures
181 examined.

182 Given our results at the brain-wide and major brain structure levels, we next determined the
183 effects of 5XFAD genotype and PTZ kindling on AT8+ pathology at the subregion level both
184 ipsilateral and contralateral to tau injection site (Fig 1E, S3, Table S1). Using Bayesian models,
185 we compared EMMs (posterior means) to determine group level differences in subregions

186 where credible genotype, treatment, or interaction effects were found (Table S1). In the
187 isocortex, we observed increased AT8+ levels in both PTZ and Sal treated 5X-TRAP mice
188 compared to WT-TRAP mice across several ipsilateral and contralateral subregions. We also
189 found that PTZ treated 5X-TRAP mice had higher AT8+ levels compared to Sal treated 5X-
190 TRAP, including in the ipsilateral somatosensory cortex, the contralateral somatosensory,
191 auditory, anterior cingulate, as well as dorsal retrosplenial and posterior parietal areas (Fig 1E,
192 S3, Table S1). PTZ treatment also increased AT8+ levels in WT-TRAP mice in the ipsilateral
193 secondary motor and contralateral anterior cingulate areas. In the hippocampus, 5XFAD
194 genotype drove increased AT8+ levels in the ipsilateral dentate gyrus (DG) and in several
195 subregions contralaterally (Fig 1E, S3, Table S1), with little change due to PTZ treatment. In the
196 thalamus, we found credible increases in AT8+ levels in 5X-TRAP mice compared to WT-TRAP
197 across several subregions. PTZ kindling resulted in increased AT8+ levels in 5X-TRAP mice in
198 several dorsal, ventral, and medial thalamic nuclei, particularly in the contralateral hemisphere,
199 and in bilateral anterior thalamic nuclei in WT-TRAP mice (Fig 1E, S3, Table S1). In the fiber
200 tracts, 5X-TRAP mice showed increased AT8+ levels compared to WT-TRAP in both
201 hemispheres, and PTZ treatment increased AT8+ levels contralaterally in 5X-TRAP and
202 bilaterally in WT-TRAP mice (Fig 1E, Table S1), suggesting a trans-neuronal mechanism in
203 increased AT8+ levels found due 5XFAD genotype and PTZ. Effects in the cortical subplate,
204 striatum, hypothalamus, pallidum, and midbrain were largely driven by 5XFAD genotype and
205 exacerbated by PTZ in select subregions (Fig 1E, Table S1). Overall, our AT8 mapping data
206 demonstrate increased tau spread due to 5XFAD genotype brain wide. In WT-TRAP mice, PTZ
207 worsened tau spread in select cortical and thalamic subregions and fiber tracts. In 5X-TRAP
208 mice, PTZ kindling worsened tau spread in subregions in the majority of major brain structures,
209 typically in the contralateral hemisphere, demonstrating that seizures drove tau spread to distal
210 (from AD-tau injection) brain regions, which otherwise have little pathology at this stage (16).
211 Taken together, these data support a causal role for seizures in enhancing the spread of tau.

212 Given we observed neuronal hyperactivity brain-wide and in major brain structures in 5X-TRAP
213 mice, we next examined the effects of 5XFAD genotype and PTZ kindling on counts of tdT+
214 neurons at the subregion level (Fig 1F, S3, Table S2). In the isocortex, we found credible
215 elevations in tdT+ counts bilaterally in PTZ treated WT-TRAP and 5X-TRAP compared to Sal
216 treated mice in the majority of subregions, including the motor, somatosensory, auditory, and
217 agranular insular areas (Fig 1F, Table S2). We also found increased tdT+ counts in PTZ treated
218 5X-TRAP mice compared to PTZ treated WT-TRAP, in these cortical subregions. PTZ kindling
219 increased tdT+ counts in the dentate gyrus of the hippocampus, with little change due to
220 genotype (Fig 1F, S3, Table S2). In the thalamus, we observed increased tdT+ counts in
221 several dorsal, ventral, and medial nuclei, where PTZ treated WT-TRAP mice showed increased
222 tdT+ counts in select regions, and PTZ kindled 5X-TRAP mice showed increased tdT+ counts
223 compared to all other groups in most of these subregions (Fig 1F, S3, Table S2). In addition, Sal
224 treated 5X-TRAP mice showed credibly increased tdT+ counts compared to Sal treated WT-
225 TRAP across several thalamic nuclei (Fig 1F, S3, Table S2). Effects in the olfactory areas,
226 cortical subplate, pallidum, hypothalamus, and midbrain were largely driven by interactions
227 between 5XFAD genotype and PTZ kindling (Fig 1F, Table S2), similar to the isocortex and
228 thalamus. In addition, genotype effects were found in several striatal subregions with increased
229 tdT+ levels found in PTZ and Sal treated 5X-TRAP mice compared to WT-TRAP (Fig 1F, Table
230 S2). Overall, our tdT+ mapping data demonstrate increased tdT+ labeling due to PTZ induced
231 seizures in circuits relevant to AD, including limbic and thalamocortical networks. These data
232 also demonstrate basal neuronal hyperactivity and increased PTZ induced neuronal
233 hyperactivity in 5X-TRAP mice.

234 When taken together, our mapping data demonstrate that regions with increased relative AT8+
235 levels tended to be hyperactive (increased tdT+ counts) in both Sal and PTZ treated 5X-TRAP
236 mice (Fig 1, S3, Table S2, S3, S4). Of note, PTZ kindled 5X-TRAP mice showed increased

237 AT8+ levels in the contralateral intralaminar nuclei of the dorsal thalamus (rhomboid, central
238 medial, paracentral, and parafascicular nuclei) of the thalamus and prefrontal areas (anterior
239 cingulate, agranular insula), which are areas where we also found credibly increased levels of
240 tdT+ counts, has previously been shown to be activated by PTZ (41, 42), and are highly
241 interconnected, demonstrating that seizures drive tau spread through hyperactive networks. Sal
242 treated 5X-TRAP mice also showed increased tau spread in areas with basal hyperactivity
243 compared to Sal treated WT-TRAP, including in striatal and thalamic subregions. These data
244 establish the first causal evidence that neuronal hyperactivity promotes tau spread preferentially
245 through hyperactive networks.

246 To determine whether sex may influence tau spread and activity dependent labeling, we
247 included sex as an independent variable in multiple linear regressions for AT8+ and tdT+ levels
248 in all major brain structures examined (Table S3). We found that female sex was associated
249 with AT8+ levels in the ipsilateral and contralateral hippocampi and ipsilateral fiber tracts. In
250 contrast, sex had a less pronounced effect on tdT+ counts, but was found to be a predictor in
251 the ipsilateral olfactory areas with elevations found in males. These results suggest that female
252 sex is associated with increased tau spread, but these effects occurred independently of
253 neuronal hyperactivity.

254 Worsened seizure severity is associated with increased tau spread
255 and activity-dependent labeling

256 As we have previously shown that 5XFAD mice have increased seizure susceptibility (24), we
257 determined whether these effects were present in AD-tau seeded 5X-TRAP mice and whether
258 seizure severity during the earlier kindling was correlated with AT8+ and tdT+ counts brain-wide
259 (Fig 2, S5, S6, S7, S8). We performed PTZ kindling and activity-dependent labeling 2-3 weeks
260 following AD-tau injection (3.5 – 4 months of age) (Fig 1B) and found that 5X-TRAP mice had

261 significantly worsened seizure severity compared to WT-TRAP, measured by daily maximal
262 Racine score and area under the curve (AUC) on the final day of PTZ administration (Fig 2A, B,
263 C), confirming our prior report (24).

264 Given our mapping data providing causal evidence that seizures enhance tau spread, we
265 performed Pearson correlations between Racine AUC and regional AT8+ levels in PTZ kindled
266 WT-TRAP and 5X-TRAP mice to determine whether seizure severity was associated with tau
267 spread (Fig 2D, 2E, S5, S6). We found several significant positive correlations between seizure
268 severity (Racine AUC) and AT8+ levels in both WT-TRAP and 5X-TRAP mice, largely in
269 thalamocortical networks (Fig 2D, 2E, S5, S6). These data further indicate a critical role of
270 seizures in enhanced tau spread, particularly in bilateral thalamocortical brain regions.

271 Next, since our prior work demonstrated associations between hippocampal activity dependent
272 labeling and seizure severity (36), we performed Pearson correlations between seizure severity
273 and tdT+ counts in 5X-TRAP and WT-TRAP mice (Fig S7, S8). We found significant positive
274 correlations largely in cortical subregions (Fig S7, S8), demonstrating that seizure severity is
275 associated with elevated activity dependent labeling.

276 Tau spread and neuronal hyperactivity are correlated with worsened 277 memory in PTZ kindled 5X-TRAP mice

278 All WT-TRAP and 5X-TRAP underwent the novel object recognition (NOR), contextual fear
279 conditioning (CFC), and open field behavioral assays at 5 – 6 months of age (Fig 1B). In the
280 NOR paradigm, the % time spent with the novel object as compared to the familiar object was
281 significantly decreased in PTZ kindled 5X-TRAP mice compared to Sal treated 5X-TRAP and
282 WT-TRAP mice (Fig 3A), demonstrating memory deficits in this group. CFC testing at 1 day
283 (recent memory) and 14 days (remote memory) following conditioning revealed no differences

between groups in recent or remote recall (Fig S9). In the open field assay, we observed decreased rearing behavior in 5X-TRAP mice, overall, compared to WT-TRAP, suggestive of decreased exploratory behavior and motor activity (Fig 3B), but the total distance traveled and the time spent in the center of the arena, a measure of anxiety-like behavior, were similar across all groups (Fig 3B). Female sex was associated with decreased rearing behavior in the open field assay, while no effects of sex or cohort were found on NOR or CFC (Table S3, S4). These results demonstrate that seizures significantly worsen memory in AD-tau seeded 5X-TRAP mice.

To determine the associations between tau spread and neuronal hyperactivity on cognition, we performed Pearson correlations between NOR performance and regional AT8+ levels and tdT+ counts in PTZ kindled 5X-TRAP mice (Fig 3C, D, S10, S11). We found strong inverse correlations between % time spent with novel object and AT8+ levels extensively throughout the brain, including in the ipsilateral intralaminar nuclei of the dorsal thalamus and agranular insular area, and in the contralateral intralaminar nuclei of the dorsal thalamus, as well as bilateral amygdalar, striatal, and hypothalamic nuclei and fiber tracts (Fig 3C, S10). Notably, many of these regions are areas in which we found elevated tau spread in PTZ kindled 5X-TRAP mice (Fig 1E, Table S1). In addition, we found that decreased NOR performance was significantly correlated with tdT+ counts in the ipsilateral hippocampal subfields, bilaterally in the intralaminar nuclei of the thalamus, prefrontal areas (agranular insula and motor), and in striatal and hypothalamic nuclei of PTZ kindled 5X-TRAP mice (Fig 3D, S11). These results demonstrate that seizure-driven exacerbation of tau spread and neuronal hyperactivity, particularly in thalamocortical circuits, are strongly associated with memory deficits in 5X-TRAP mice.

Network dynamics of tau spread are altered by 5XFAD genotype and seizure induction

308 Given our data demonstrating increased tau propagation in PTZ kindled and 5X-TRAP mice, we
309 next employed well-validated computational models (19, 43) to study whether 5XFAD genotype
310 or PTZ kindling impacted the pattern of tau spread between brain regions. Prior studies using
311 computational modeling of tau pathological progression have demonstrated that tau spreads
312 throughout the brain via the neuroanatomical connectome, predominantly in a retrograde
313 direction (19). We implemented linear diffusion models of tau spread from AD-tau injection sites
314 (hippocampal and posterior parietal association area (PTLp) seeds) along a network defined by
315 either anterograde connectivity, retrograde connectivity, or Euclidean (geometric) distance
316 between brain areas derived from Oh and colleagues (44). We then compared the performance
317 of each of these spread models in predicting regional AT8+ levels from each experimental
318 group (Fig 4, S12).

319 Consistent with prior data (19), we found that retrograde models tended to outperform
320 anterograde and Euclidean models (Fig 4A-C, Fig S12). However, anterograde models
321 produced a statistically significant fit with 5X-TRAP mice but not with WT-TRAP mice (Fig 4A). A
322 model combining anterograde, retrograde, and Euclidean distance called “Bidirectional
323 Euclidean” fit better than any individual model in all groups (Fig S12). To further examine the
324 relative importance of anterograde, retrograde, and Euclidean tau spread, we compared
325 standardized regression beta weights from the “Bidirectional Euclidean” model (Fig S12)
326 between groups, which provide a quantitative measure of the relative importance of each mode
327 of spread to the overall model fit (Fig 4D). We found that anterograde beta weights (Fig 4D) and
328 anterograde: retrograde and anterograde: Euclidean beta weight ratios (Fig 4E) were increased
329 in Sal treated 5X-TRAP mice compared to WT-TRAP, suggesting that anterograde connectivity
330 specifically has an increased contribution to tau spread in 5X-TRAP mice relative to WT-TRAP
331 mice. Beta weights were similar between PTZ and Sal treated 5X-TRAP mice (Fig 4D).
332 Retrograde betas were lower in PTZ kindled 5X-TRAP mice compared to Sal treated WT-TRAP

333 mice, while Euclidean spread betas were lower in Sal treated 5X-TRAP compared to all other
334 groups (Fig 4D). To confirm the regional specificity of the model, we repeated the retrograde
335 spread modeling in WT-TRAP mice using 500 random seed sites with similar spatial clustering
336 to the seed sites (i.e. the dorsal hippocampus and posterior parietal association area (PTLp)).
337 We found that the model performance with the experimental seed site was better than 99% of
338 the randomly chosen seed sites (Fig S13). In addition, we implemented linear diffusion models
339 using hippocampus only and PTLp only seed sites (Fig S14). In general, the hippocampal model
340 recapitulated the dual seed site model, while the PTLp model performed poorly, suggesting that
341 the hippocampus is the primary seed site for tau spread across our experimental groups.
342 Overall, these computational analyses show that all groups fit with a pattern of connectome-
343 based spread and that primarily anterograde spread contributes to the elevations in AT8+ levels
344 quantified in our brain mapping data in Sal and PTZ treated 5X-TRAP mice (Fig 1).

345 Regional neuronal activity levels at 4 months of age are predictive of
346 tau spread at 6 months of age

347 Given that we have established a causal role of seizures in elevated tau spread in 5X-TRAP
348 mice and that elevations in tau pathology tended to occur in hyperactive brain regions, we next
349 determined whether tdT+ counts were predictive of tau spread. To do so, we correlated regional
350 counts of tdT+ neurons with detected AT8+ immunoreactive aggregates while accounting for
351 predicted Bidirectional Euclidean spread (Fig 5). We found significant positive relationships
352 between tdT+ counts and relative AT8+ levels in Sal treated WT-TRAP mice, demonstrating that
353 basal neuronal activity is predictive of tau spread. tdT+ counts were not predictive of relative tau
354 spread in PTZ treated WT-TRAP mice, since PTZ increased tdT+ counts with relatively little
355 change in AT8+ levels in these mice (Fig 1, S3, Table S1, S2). Additionally, tdT+ counts were
356 predictive of tau spread in Sal treated 5X-TRAP mice, suggesting that basal hyperactivity found

357 in Sal treated 5X-TRAP mice contributes to increased tau spread. A positive relationship
358 between tdT+ counts and AT8+ levels was also found in PTZ treated 5X-TRAP mice, further
359 strengthening the causal role of neuronal hyperactivity in tau spread established in this group.
360 Overall, given that activity dependent labeling took place soon after tau seeding (prior to
361 extensive tau spread (16, 19) (Fig 1B)), these data demonstrate a preferential vulnerability of
362 hyperactive circuits to tau propagation, and provide additional evidence of hyperactivity driven
363 tau spread in 5X-TRAP mice.

364 Hyperactive neuronal populations labelled at 4 months of age are 365 more likely to exhibit tau pathology than surrounding neurons at 6 366 months of age

367 Given our results establishing that tau spreads via hyperactive networks in 5X-TRAP mice, we
368 next determined whether hyperactive neurons accumulate more pathological tau. We examined
369 whether tdT+ neurons were more likely to develop somatic AT8+ immunoreactivity compared to
370 surrounding tdT- (NeuN+) neurons. Detected and mapped tdT+ and tdT- (NeuN+) neurons were
371 colocalized with detected AT8+ immunoreactive aggregates across all sampled brain regions to
372 calculate the percentage of tdT+ and tdT- neurons with somatic tau pathology in 5X-TRAP (Fig
373 6) and WT-TRAP (Fig S15) mice. Ipsilaterally, we found increased AT8+ colocalization with
374 tdT+ neurons compared to tdT- in Sal treated 5X-TRAP mice in the isocortex, cortical subplate,
375 striatum, and thalamus and increased AT8+ colocalization in tdT+ neurons compared to tdT- in
376 PTZ kindled 5X-TRAP mice in the striatum and thalamus. In the contralateral hemisphere, we
377 found that tdT+ neurons were more likely to colocalize with AT8 immunoreactivity than
378 surrounding tdT- neurons in the thalamus of PTZ kindled 5X-TRAP mice (Fig 6). Given our
379 results showing increased AT8+ levels and high tdT+ counts in the cortex of PTZ treated 5X-
380 TRAP mice, we expected to see increased tdT+ colocalization with AT8 in the cortex, but we

found no differences in these mice. These results are likely due to increased neuronal death (Fig S16) in seizure activated cortical neurons carrying a high tau load. In contrast, WT-TRAP mice did not exhibit any significant differences in AT8 colocalization due to kindling or tdT labelling (Fig S15). In summary, both Sal and PTZ treated 5X-TRAP mice exhibited increased tau pathology in tdT+ neurons compared to tdT- neurons in regions with increased overall AT8+ levels and tdT+ counts, demonstrating that seizure and basally hyperactive populations disproportionately contribute to tau spread in these mice.

Human postmortem AD brains exhibit increased tau pathology in association with a history of seizures

To determine whether seizures worsen indications of tau spread in AD, we analyzed postmortem pathological ratings across 18 brain regions from AD patients and stratified subjects based on the presence or absence of clinical seizure history. We found that AD patients with clinical seizure history (AD+Sz) exhibited more severe tau pathological ratings (phosphorylated tau (Ser396/404); PHF1 antibody) compared to AD patients without a clinical seizure history (AD-Sz). We found these alterations in regions affected at late Braak stages, the angular gyrus and a strong trend in the middle frontal gyrus (Fig 7). We did not find significant differences in regions involved in early Braak stages including the locus coeruleus and entorhinal cortex (Fig 7). We additionally performed ordinal linear regressions and found that male sex was associated with increased tau pathology in the substantia nigra and locus coeruleus (Table S5). These patterns indicate that a history of seizures is associated with increased tau pathology in brain regions impacted at advanced disease stages in AD, supporting our causal evidence that seizures increase tau spread in 5X-TRAP mice.

Discussion

404 Our study demonstrates for the first time that neuronal hyperactivity increases pathological tau
405 spread through interconnected brain regions in an AD model. Our data also highlight that tau
406 preferentially spreads through hyperactivated brain networks and neuronal populations in the
407 anterograde direction in 5X-TRAP mice. Further, we found that tau spread and neuronal
408 hyperactivity are highly and extensively correlated with worsened memory caused by seizures.
409 We found corroborating data in postmortem human AD brain tissue, suggestive of increased tau
410 spread in patients with a history of seizures. Together, our data demonstrate hyperactive
411 networks and neurons as therapeutic targets to slow AD progression.

412 TRAP models are widely used in basic research and our recent work demonstrated that tdT
413 labelling during seizure induction allows for the long-term tracking of hyperactive neuronal
414 populations (36). Here we report the development of a novel model involving the cross of these
415 mice with a neurodegenerative mouse. With tamoxifen-inducible, neuronal activity (Fos) driven
416 labeling, the 5X-TRAP model can be used to examine the interactions between neuronal activity
417 and AD pathology. For these studies, we used the 5X-TRAP mouse in conjunction with AD-tau
418 seeding and PTZ seizure kindling as a robust model to test our hypothesis that neuronal
419 hyperactivity drives subsequent tau spread and to determine the contribution of activated
420 networks and neuronal populations to tau spread.

421 Prior studies have demonstrated that induced neuronal activity can worsen endogenous
422 pathology in a tauopathy model (17). Here, using a tau seeding paradigm, we provide the first *in*
423 *vivo* evidence of a causal relationship between neuronal hyperactivity, through seizure
424 induction, and increased tau spread in mice that otherwise lack overt phospho-tau pathology
425 (16, 39). In addition, we show that injection of pathological tau in the mouse brain recapitulates
426 aspects of the connectome-directed propagation observed in human AD (13, 19). We performed
427 AD-tau seeding unilaterally in the right dorsal hippocampus and overlying cortex (posterior
428 parietal association area), as prior studies have shown robust tau spread following seeding at

429 these sites (13, 16, 19). In contrast, tau seeding in the locus coeruleus, the earliest region
430 impacted in AD, results in limited spread, with the hippocampus and entorhinal cortex largely
431 spared of tau pathology (45, 46). Following AD-tau seeding, mice underwent PTZ seizure
432 induction or control (saline) administration and all seizure or basally activated neurons labeled
433 with tdT using the TRAP methodology. We found that 4 month old 5X-TRAP mice show basal
434 increases in activity-dependent tdT labeling, corroborating prior reports of hyperexcitability in
435 amyloidosis models (28, 47), which may underlie increased seizure susceptibility in 5XFAD (24)
436 and 5X-TRAP mice.

437 For an unbiased approach to measure the spread of tau, we performed comprehensive
438 brain mapping on sectioned tissue from AD-tau seeded WT-TRAP and 5X-TRAP mice. First, we
439 found that Sal treated 5X-TRAP mice had significantly increased tau spread in cortical and
440 subcortical regions and fiber tracts, relative to WT-TRAP mice, expanding upon prior reports of
441 increased spread in amyloidosis models, including 5XFAD mice (15, 16). Next, we observed
442 that PTZ kindling caused further increases in tau spread in 5X-TRAP mice in several cortical
443 regions, the thalamus, striatum, and fiber tracts. The majority of PTZ driven effects in 5X-TRAP
444 mice were found contralateral to tau injection, demonstrating that seizures drove tau spread to
445 regions that would otherwise have minimal pathology at this stage (3 months post seeding) (16).
446 In both PTZ and saline-treated 5X-TRAP mice, regions with high tdT counts tended to be
447 associated with relative increases in tau pathology. PTZ induces thalamocortical seizure activity
448 (41, 42), and our data show increased spread particularly in hyperactive interconnected regions
449 of the thalamus and cortex, such as intralaminar nuclei of the dorsal thalamus and prefrontal
450 regions, and in fiber tracts. These data suggest that seizure induced hyperactivity (increased
451 tdT+ counts) drives axonal transport and tau spread through activated networks.

452 Thalamocortical Ttau spread in 5X-TRAP mice was associated with worsened cognitive
453 performance in the NOR task, consistent with human studies linking cognitive decline and tau

454 progression in AD (7-10). Of note, we did not find significant differences in CFC, which may
455 indicate a selective deterioration of circuit function. CFC is largely mediated by the amygdala
456 and hippcompus, while NOR is cortically driven. These behavioral data further establish a role
457 of seizure-induced tau spread in overall disease progression.

458 PTZ kindled WT-TRAP mice also showed increased tau spread through thalamocortical
459 networks and fiber tracts, consistent with seizure driven spread through activated circuits.
460 However, compared to 5X-TRAP mice, PTZ kindling had relatively little effect on tau pathology
461 in WT-TRAP mice. One plausible explanation for this may be that interactions between Aβ and
462 neuronal hyperactivity promote enhanced seeding effects. Notably, we have found that PTZ
463 kindling increases Aβ pathology in 5XFAD mice (24), which in turn can further increase and
464 promote sustained hyperactivity, creating a positive feedback loop (32), which may result in
465 exacerbated tau spread. Indeed, amyloid-related hyperconnectivity was recently associated with
466 tau spread in AD (14). A second explanation is that WT-TRAP mice had significantly reduced
467 seizure severity compared to 5X-TRAP mice. Future studies should continue kindling in WT-
468 TRAP mice until similar levels of tonic-clonic seizures are achieved to determine whether
469 increased seizure severity could increase tau spread in WT mice. Together, our mapping data
470 suggest that Aβ and neuronal hyperactivity interactions promote the spread of tau in 5X-TRAP
471 mice.

472 Notably, we found a significant effect of female sex on increased tau spread in mice, although
473 similar changes were not found in our human cohort. This may indicate that effects of sex on tau
474 spread may be dependent on disease severity, as these cases were late-stage. Indeed, our
475 results in mice are consistent with tau positron emission tomography (PET) studies in patients
476 with mild to moderate cognitive impairment due to AD, in which females had accelerated tau
477 propagation (48, 49). Our data do not suggest that sex effects on tau spread in mice are due to
478 changes in neuronal hyperactivity as we found little difference between males and females in

479 seizure severity or tdT labeling. However, since we have previously demonstrated that female
480 5XFAD mice had increased Aβ plaques and mTORC1 activation compared to males (24), it is
481 plausible that increased tau spread in females found here may be due to increased neuritic
482 plaque tau or a reduction in autophagy, caused by elevated mTOR activity (50), resulting in
483 increased intracellular tau accumulation.

484 To determine whether genotype or seizure induction altered the patterns of tau spread, we
485 utilized connectomic data made available from the Allen Institute (44). Consistent with prior
486 results (19), models incorporating anterograde, retrograde, and Euclidean distance-based
487 spread had better fit with measured AT8+ levels than any model individually. These data are
488 indicative, overall, of a connectome driven spread of tau, which is further supported by our
489 findings of high AT8+ levels in fiber tracts, particularly in PTZ treated 5X-TRAP mice. These
490 models also indicate that, while we used two seed sites, the hippocampus was the primary initial
491 site of tau seeding effects. From the dual seed site analyses, measured AT8+ levels in PTZ
492 treated 5X-TRAP and WT-TRAP mice tended to have worse fit with anterograde and retrograde
493 models, compared to their Sal treated counterparts, which may be indicative of altered
494 anatomical and functional long-range connectivity (reducing fit with a standardized connectomic
495 dataset) and enhanced local connectivity caused by seizures (51-54). We also found that
496 measured AT8+ levels in 5X-TRAP mice, but not WT-TRAP, fit with anterograde models of
497 spread. Indeed, compared to anterograde, we found lower relative contribution of Euclidean and
498 retrograde models to spread in Sal and PTZ treated 5X-TRAP mice, respectively. When taken
499 with our mapping data, these results suggest that increased AT8+ levels in 5X-TRAP mice are
500 primarily due to increased anterograde spread.

501 We next used these connectome-based models to further link neuronal activity to tau spread.
502 We found that regional neuronal activity levels (tdT+ counts) were predictive of relative tau
503 spread in all groups except PTZ treated WT-TRAP mice. The lack of an effect in PTZ treated

504 WT-TRAP mice was expected since there was increased tdT+ counts due to seizure induction
505 with relatively little change in tau spread. The relationship between neuronal activity level and
506 predictivity of tau spread in Sal treated WT-TRAP mice suggest that tau preferentially travels
507 between basally active networks. Similarly, tau has been shown to spread through the default
508 mode network in human patients, which are more metabolically active at rest (1, 4, 6). Our
509 results also indicate that regional neuronal activity levels are predictive of relative tau levels in
510 5X-TRAP mice, further suggesting that neuronal hyperactivity drives increased tau spread in
511 these mice, demonstrating a vulnerability of hyperactive networks to tau propagation.

512 Another novel aspect of our study was the ability to specifically label and track hyperactivated
513 neuronal populations to determine their contribution to tau spread months after their original
514 activation. We found that tdT+ neurons were more likely to colocalize with AT8 than the
515 surrounding tdT- neurons in the thalamus and striatum of both PTZ and Sal treated 5X-TRAP
516 mice, indicating that these populations drove enhanced overall tau spread. Increased pathology
517 found in these populations may also be associated with increases in tau kinases, as seen in
518 temporal lobe epilepsy (29). TRAP labeling utilizes cFos as a proxy marker of neuronal activity
519 limiting the temporal precision of neuronal dynamics. While elevated tdT+ levels indicate early
520 population hyperactivity and we have previously demonstrated sustained hyperexcitability in
521 seizure-activated neurons (36), the mechanisms underlying cellular hyperexcitability in tdT+ 5X-
522 TRAP neurons remain to be explored. Nevertheless, the ability to label and track these
523 populations provides a robust framework through which mechanistic studies may be performed
524 to identify the pathophysiological alterations that underlie tau propagation in these vulnerable
525 populations to identify therapeutic targets to slow tau spread.

526 To expand our investigations of the role of neuronal hyperactivity in tau pathology distribution in
527 human AD, we performed a retrospective analysis of postmortem tau pathological ratings brain-
528 wide. We found changes consistent with increased tau spread in AD patients with seizure

529 history compared to those without, consistent with a clinical study demonstrating that the
530 development of seizures in AD is associated with increased CSF tau levels (55). While clinical
531 examination of the relationship between seizures and tau localization in the brain is limited, a
532 recent study from Lam and colleagues (56) found associations between seizure foci and spatial
533 development of both tau and amyloid pathology, additionally corroborating our results that
534 neuronal activity levels were predictive of tau spread in that region. These data suggest that
535 there may be clinical value in screening AD patients for epileptiform activity or other
536 electrographic biomarkers, along with tracking tau progression by PET.

537 Overall, our data support neuronal hyperexcitability as a target to slow AD progression,
538 especially early in the disease. Indeed, the antiseizure medication (ASM), levetiracetam, slowed
539 cognitive decline in mild cognitive impairment (57) and AD patients with epileptiform activity
540 (58), but both studies used short term treatments (≤ 4 weeks) and did not examine pathological
541 progression. Based on our results, studies with long term ASM therapy and serial tau PET
542 scans would be warranted to link seizure control with modulation of tau spread. Other drugs
543 targeting hyperexcitability may also hold promise. Indeed, we have found that modulating
544 network dysfunction via inhibition of mTORC1 activity with rapamycin reduced Aβ and cognitive
545 deficits in PTZ kindled 5XFAD mice (24).

546 Together, these studies indicate that in the presence of Aβ, neuronal hyperactivity promotes
547 anterograde tau spread through hyperactive networks and neurons, with rates of tau spread
548 associated with cognitive dysfunction. Thus, we contribute to a model of AD progression
549 whereby amyloid-neuronal hyperactivity interactions enhance the spread of tau, advancing
550 disease progression and cognitive decline, a process which is exacerbated by seizures (Fig 8).
551 Targeting neuronal hyperactivity, particularly at early, Aβ-predominant stages in AD, should be
552 prioritized to slow overall disease progression.

553 # Methods

554 ## Mice

555 All mouse procedures and protocols were approved by the University of Pennsylvania
556 Institutional Animal Care and Use Committee (IACUC) Office of Animal Welfare. Fos$^{2A\text{-}iCreER}$
557 (TRAP2) and B6.Cg-*Gt(ROSA)26Sor*$^{tm14(CAG\text{-}tdTomato)Hze}$/J (Ai14) were obtained from Jackson
558 Laboratory (stock 030323, 007914). TRAP2 and Ai14 mice were crossed for two generations,
559 producing mice homozygous for Fos$^{2A\text{-}iCreER}$ and B6.Cg-*Gt(ROSA)26Sor*$^{tm14(CAG\text{-}tdTomato)Hze}$/J.
560 5XFAD on a mixed B6SJL background first generation (F1) generated from mice purchased
561 from Jackson Laboratory (MMRRC strain #034840, Bar Harbor ME) were bred with mice
562 homozygous for TRAP2/Ai14 to produce 5XFAD x TRAP (5X-TRAP) and littermate WT x TRAP
563 (WT-TRAP) experimental mice that were used in all biochemical and behavioral experiments.
564

565 ## AD-tau isolation

566 AD-tau isolation was performed as previously established (13) from cortical tissue from patients
567 confirmed to have AD by neuropathological diagnosis. Total protein concentrations were
568 determined by BCA and tau, Aβ, and alpha synuclein concentrations were determined by
569 ELISA: purified tau= 0.4-1.1 μg/μL, $A\beta_{42}$ = 32-132 ng/mL, $A\beta_{40}$ =3-46 ng/mL, and α synuclein=
570 nondetectable – 0.54 μg/mL.
571

572 ## Stereotaxic surgery

573 AD-tau was injected into 3-month-old mice using previously established protocols (16). Briefly,
574 mice were anesthetized with ketamine-xylazine-acepromazine (90 mg/kg, 10 mg/kg, 2 mg/kg)
575 and mounted in a stereotaxic apparatus. A hole was bore from 2.5 mm posterior from Bregma
576 and 2.0 mm lateral (right) from midline. A Hamilton syringe was lowered 2.4 mm and 2.5 μL of

577 0.4 μg/μL (1 μg) AD-tau was injected into the dorsal hippocampus. The syringe was then
578 retracted 1 mm (1.4 mm depth) and an additional 1 μg of AD-tau was injected into the posterior
579 parietal association area. An example of tau injection sites can be found in Figure S4.
580

581 ## PTZ kindling

582 Two to three weeks following AD-tau injection, mice underwent PTZ kindling using previously
583 established protocols (24, 28). Briefly, mice were injected (I.P.) every 48 hours for 15 days (8
584 injections) with 35 mg/kg PTZ (Sigma Aldrich, St Louis MO) or vehicle (0.9% saline, Sigma-
585 Aldrich). Mice were monitored and video-recorded for 45 minutes after PTZ administration and
586 Racine scored for seizure severity. We used a modified Racine score (ref): 0=normal behavior,
587 1=freezing, 2=hunching with facial automatism, 3=rearing and forelimb clonus, 4=rearing with
588 forearm clonus and falling, 5=tonic-clonic seizure, 6=death. To minimize death, mice received
589 31.5 mg/kg PTZ following a stage 5 seizure and if mice reached three consecutive days of stage
590 5 (tonic-clonic) seizures, they underwent one additional PTZ treatment and were then removed
591 from kindling. To generate area under the curve (AUC) for seizure activity, we used the maximal
592 score reached per minute over 15 minutes following the final PTZ administration.
593

594 ## 4-OHT administration

595 5X-TRAP and WT-TRAP mice were injected with 4-hydroxytamoxifen (50 mg/kg, I.P.) to induce
596 permanent tdTomato expression in neurons that were activated (Fos-expressing) in the 4-6 hour
597 window after administration. AD-tau seeded 5X-TRAP and WT-TRAP mice were injected with 4-
598 OHT 30 min prior to the final PTZ or saline treatment to induce tdTomato expression in seizure
599 or basally activated (Fos expressing) neurons (36).
600

601 ## Mouse behavior

602 Behavioral experiments were carried out in the Neurobehavior Testing Core in the Translational
603 Research Center at the University of Pennsylvania. Experimenters were blind to genotype and
604 condition. Mice underwent a behavioral battery consisting of the open field assay, NOR, and
605 CFC. Procedures took place from 5 – 6 months of age in all WT-TRAP and 5X-TRAP mice.
606 Mice that were single housed were excluded from NOR and CFC.
607
608 *Open field assay*. Spontaneous locomotion and rearing activity were assessed in an open field
609 arena (14” x 14” x 18”). The Photobeam Activity System (San Diego Instruments) was used to
610 acquire data. The arena is fitted with a scaffold of IR emitters and detectors to collect peripheral,
611 center and vertical (rearing) beam breaks. After a thirty-minute habituation to the testing room, a
612 ten-minute trial began with a mouse placed in the center of the arena. All trials were recorded by
613 high-definition camcorders. Digitally recorded trials were processed for automated analysis by
614 ANYmaze software (Stoelting Co, Il) to obtain additional measures.
615
616 *Novel object recognition*. The novel object recognition procedure consisted of habituation/pre-
617 exposure, acquisition and recall trials. Before habituation, mice were handled daily for two
618 minutes for three consecutive days. The habituation/pre-exposure phase consists of daily five-
619 minute trials where the mouse is allowed to freely explore the empty NOR arena (approx. 1
620 square foot). During the acquisition trial, mice are returned to an arena containing a pair of the
621 same objects. The object pairs used are either glass bottles or metal bar (2”x 2” x five”) placed
622 about three inches from the arena walls. Mice freely explore the object pairs for fifteen minutes.
623 The arena and objects are cleaned with 70% EtOH between all trials. 24 hours after acquisition,
624 mice returned to the arena, with one of the now-familiar objects replaced with a novel object (for
625 example a bottle may be swapped with a metal bar or vice versa). During the recall trial, mice
626 explore the two objects for 15 minutes. All trials are digitally recorded for automated off-line
627 grading by ANYmaze software (Stoelting Co, Il). Time spent exploring (approaches and sniffing)

628 and was determined as the primary dependent variable. Mice that did not explore each object
629 for a minimum of 10 seconds during learning and recall were excluded from analysis.
630
631 *Contextual fear conditioning.* Mice were habituated to experimenter handling for three days prior
632 to acquisition. For acquisition, mice were placed in a soundproof conditioning chamber (Med
633 Associates, Fairfax, VT) for 4.5 minutes, during which time they received to unsignaled foot
634 shocks (1 mA, 2s) at 1-minute intervals. For recall trials, mice were returned to the conditioning
635 chamber for 5 minutes at 1 day (recent memory) and 14 days (remote memory) after
636 acquisition, without any stimulation. Behavior was recorded during all trials and freezing
637 behavior (lack of movement except for breathing) was assessed with FreezeScan software
638 (Clever Systems, Reston, VA). Results from recall trials were analyzed relative to baseline
639 freezing levels while the mice were in the recording chamber prior to foot shock during the
640 acquisition trial to control for baseline differences in freezing behavior.
641

642 Euthanasia

643 Mice were anesthetized by I.P. injection of pentobarbital (50 mg/kg) (Sagent Pharmaceuticals,
644 Schaumburg, IL) and underwent cardiac perfusion with ice cold 4% paraformaldehyde.
645

646 Immunohistochemistry

647 Brains were incubated at 4ºC for 24 h in 4% PFA, followed by sequential incubations in 10%,
648 20%, and 30% sucrose at 4ºC. Samples were then cryoprotected in OCT Tissue Tek and
649 sectioned at 20 µm. Immunohistochemistry (IHC) was performed using standard, previously
650 published protocols (24). Briefly, slices were permeabilized (0.02% triton-X100 in PBS) for 30
651 minutes, blocked for 1 hour (5% normal goat serum, 0.01% triton X-100, 1% bovine serum
652 albumin), and incubated with primary antibody (see Table S6) in blocking solution overnight at

653 4ºC and for one hour with secondary antibodies Alexa Fluor (Thermo Fisher Scientific, Waltham
654 MA) at a concentration of 1:1000.
655
656 ## Fluorojade-B

657 Cryosectioned (20 μm) tissue was stained for fluorojade-B following manufacturer's instructions
658 (EMD Millipore, Burlington, MA). Briefly, slides were sequentially incubated in 80% ethanol for 5
659 min, 70% ethanol for 2 min, distilled water for 2 min, 0.06% KMnO4 for 15 min, distilled water for
660 2 min, 0.001% fluorojade-B solution for 20 min, and distilled water for 1 min (3 times). Images
661 were acquired using a Nikon Eclipse 80i microscope and a digital Nikon DS-Fi2 camera (Micro
662 Video Instruments, Avon MA) with a 20X objective. Fluorojade B+ cells were counted using
663 Image J.
664
665 ## Slide scanning and quantifications

666 Fluorescent slide scanning for sectioned tissue was performed with a 3DHISTECH Lamina
667 Scanner (Perkin Elmer, Waltham, MA) with a 20X objective. We used NeuroInfo software (MBF,
668 Williston, VT) to register brain slices to the Allen Brain Atlas (ABA) and detect and map tau
669 AT8+ immunoreactive aggregates and tdT+ and tdT-/NeuN+ neuronal populations. All AT8+
670 immunoreactive aggregates and tdT+ neurons were detected. Given that NeuN staining was
671 inconsistent within samples, only tdT-/NeuN+ cells with sharp, defined edges were detected
672 providing a representative sampling of tdT-/NeuN+ cells for each region. Data containing each
673 detected object were exported from NeuroInfo and analyzed in R. Each object was summed
674 through the ABA hierarchy (e. g. Somatosensory area and auditory area counts were added to
675 the isocortex counts). Brain regions that contained imperfections (e.g. folds, hole in tissue) were
676 excluded from analysis for that sample. Only brain regions with at least six samples per group
677 were included for analysis. Additionally, for cell type (tdT+/tdT-) colocalization with tau

pathology, regions were excluded in samples that did not contain at least 8 tdT+ and 8 tdT- cells. ABA heatmaps displayed in Figures 1, 2, and 3 were generated using Mouse Brain Heatmap (59).

Computational analysis

As in prior work (43), we used linear diffusion models to predict the spatial distribution of tau pathology, $\boldsymbol{x}(t)$, across *N* regions defined by the Allen Brain Atlas, using an *N* x *N* adjacency matrix $\boldsymbol{A}$, whose edge weights are the directed structural connectivity strength from region *i* to region *j.* Connectivity strength was defined by fluorescence intensity from retrograde viral tract tracing (44). We computed the estimated regional tau pathology $\hat{\boldsymbol{x}}(t)$ using an equation of the form $\hat{\boldsymbol{x}}(t) = e^{-c\boldsymbol{L}t}\boldsymbol{x}_o$, where *t* is 3 months post injection, $\boldsymbol{x}_o$ is a vector with 1 unit of pathology in the hippocampal and cortical injection sites, $\boldsymbol{L}$ is the out-degree Laplacian of $\boldsymbol{A}$, and *c* is a free parameter obtained through model fitting. The injection sites were the right dentate gyrus, CA1, CA3, and posterior parietal association area. We generated distributions of model fit, i.e. the spatial correlation between $\boldsymbol{x}(t)$ and $\hat{\boldsymbol{x}}(t)$, using bootstrapped samples of mice to compare models where $\boldsymbol{A}$ is defined by retrograde connectivity, anterograde connectivity, or interregional Euclidean distance. Finally, we used multivariate regression to construct a “Bidirectional Euclidean tdT” model which combined predicted anterograde spread, retrograde spread, and Euclidean distance-based spread from optimized models with tdT positive cell counts using the following form: $\boldsymbol{x}(t) = \beta_a\hat{\boldsymbol{x}}(t)_a + \beta_r\hat{\boldsymbol{x}}(t)_r + \beta_e\hat{\boldsymbol{x}}(t)_e + \beta_T T + \varepsilon$, where $\hat{\boldsymbol{x}}(t)_a$ is predicted anterograde spread, $\hat{\boldsymbol{x}}(t)_r$ is predicted retrograde spread, $\hat{\boldsymbol{x}}(t)_r$ is spread based on Euclidean distance, T is a vector of tdT positive cell counts, and ε is an error term. Distributions of bootstrapped model fits or regression beta weights were compared using a two-tailed non-parametric test (60).

Human subjects

All human procedures and protocols were approved by the ethical standards of the Institutional Review Board (IRB) at the University of Pennsylvania. Subjects were diagnosed with AD based on clinical history, and neurological and neuropsychological assessment. Clinical diagnoses were confirmed post-mortem based on staging of $A\beta_{42}$ and tau pathology. For assessment of tau pathology distribution in AD patients and control subjects, numeral ratings across 18 brain regions were retrieved from the Center for Neurodegenerative Disease Research (CNDR) database at the University of Pennsylvania. The frequency of tau pathology was scored by expert pathologists using a standard semi-quantitative scale: 0 (absent), 1 (sparse), 2 (moderate), and 3 (frequent). Clinical data from these patients are reported in Table S7.

Statistics

AT8+ and tdT+ mapping data were first analyzed by linear mixed models with genotype and treatment as fixed effects and brain region (subregion level) and subject as random effects and group contrasts were compared by EMM. We then performed hierarchical Bayesian modeling separately for each of the major parent brain regions (isocortex, hippocampus, cortical subplate, striatum, thalamus, hypothalamus, midbrain, and fiber tracts) incorporating subregions nested within parent regions as random effects. In major brain structures where credible genotype, treatment or genotype x treatment effects were found, we performed additional Bayesian statistical modeling with genotype, treatment, and brain subregion as fixed effects to determine genotype, treatment, and interaction effects at individual brain subregions. Where credible genotype, treatment, or genotype x treatment effects were found, we computed EMMs to determine group level differences for each identified brain region. For Bayesian statistics, credible effects and contrasts were identified when 95% credible intervals did not include 0. Results from Bayesian modeling and group contrasts can be found in Tables S1 and S2. For all

728 Bayesian models, weakly informative priors based on pilot studies were used to indicate
729 interactions between 5XFAD genotype and PTZ kindling to increase AT8+ and tdT+ levels.
730 Details of Bayesian models, including convergence and effective sample sizes can be found in
731 Table S8. Daily maximal Racine scores were compared between WT-TRAP and 5X-TRAP mice
732 by repeated measure 2-way ANOVA with PTZ administration (repeated measure) and genotype
733 (WT-TRAP vs 5X-TRAP) as independent variables with Sidak's post hoc to identify group
734 differences. Area under the curve of Racine scores were compared between WT-TRAP and 5X-
735 TRAP mice by two-tailed t-test. Behavior comparisons were made by 2-way ANOVA with
736 genotype (WT-TRAP vs 5X-TRAP) and kindling (saline vs PTZ) as independent variables with
737 Sidak's post hoc to identify group differences when main effects or interactions were found.
738 Correlations between regional AT8+/tdT+ counts and behavior were identified by Pearson
739 correlation. For AT8+ colocalization experiments (Fig 6, S15), WT-TRAP and 5X-TRAP were
740 analyzed separately by 2-way ANOVA with kindling (saline vs PTZ) and cell type (tdT+ vs tdT-)
741 as independent variables for each sampled brain region with Tukey's post hoc where main
742 effects or interactions were found. Human pathological ratings were compared by two-tailed
743 Mann-Whitney test. Males and females were included in all experiments. Sex was added as an
744 independent variable for each dataset and analyzed by multiple or ordinal linear regressions
745 and are included in Table S3 and S5. Homogeneity of variance was confirmed for all 2-way
746 ANOVA analyses. Statistical analyses for brain mapping, AT8 colocalization, and ordinal
747 regressions were performed in R (4.3.2). All other statistical analyses were performed in Prism
748 10 (GraphPad, Boston, MA). Multiple comparisons were adjusted where appropriate as
749 described above. All statistical tests were two-sided.
750

751 **Data availability**

The data that support the findings of this study are available upon reasonable request from the corresponding authors.

Code availability

The code used for computational analyses is available at https://github.com/ejcorn/tau-seizures.

References

1. Vogel JW, Iturria-Medina Y, Strandberg OT, Smith R, Levitis E, Evans AC, Hansson O, Alzheimer's Disease Neuroimaging I, Swedish BioFinder S. Spread of pathological tau proteins through communicating neurons in human Alzheimer's disease. Nat Commun. 2020;11(1):2612.
2. Schoonhoven DN, Coomans EM, Millan AP, van Nifterick AM, Visser D, Ossenkoppele R, Tuncel H, van der Flier WM, Golla SSV, Scheltens P, Hillebrand A, van Berckel BNM, Stam CJ, Gouw AA. Tau protein spreads through functionally connected neurons in Alzheimer's disease: a combined MEG/PET study. Brain. 2023;146(10):4040-54.
3. Zhou J, Gennatas ED, Kramer JH, Miller BL, Seeley WW. Predicting regional neurodegeneration from the healthy brain functional connectome. Neuron. 2012;73(6):1216-27.
4. Hoenig MC, Bischof GN, Seemiller J, Hammes J, Kukolja J, Onur OA, Jessen F, Fliessbach K, Neumaier B, Fink GR, van Eimeren T, Drzezga A. Networks of tau distribution in Alzheimer's disease. Brain. 2018;141(2):568-81.
5. Cope TE, Rittman T, Borchert RJ, Jones PS, Vatansever D, Allinson K, Passamonti L, Vazquez Rodriguez P, Bevan-Jones WR, O'Brien JT, Rowe JB. Tau burden and the functional connectome in Alzheimer's disease and progressive supranuclear palsy. Brain. 2018;141(2):550-67.
6. Franzmeier N, Rubinski A, Neitzel J, Kim Y, Damm A, Na DL, Kim HJ, Lyoo CH, Cho H, Finsterwalder S, Duering M, Seo SW, Ewers M, Alzheimer's Disease Neuroimaging I. Functional connectivity associated with tau levels in ageing, Alzheimer's, and small vessel disease. Brain. 2019;142(4):1093-107.
7. Bejanin A, Schonhaut DR, La Joie R, Kramer JH, Baker SL, Sosa N, Ayakta N, Cantwell A, Janabi M, Lauriola M, O'Neil JP, Gorno-Tempini ML, Miller ZA, Rosen HJ, Miller BL, Jagust WJ, Rabinovici GD. Tau pathology and neurodegeneration contribute to cognitive impairment in Alzheimer's disease. Brain. 2017;140(12):3286-300.
8. Xia C, Makaretz SJ, Caso C, McGinnis S, Gomperts SN, Sepulcre J, Gomez-Isla T, Hyman BT, Schultz A, Vasdev N, Johnson KA, Dickerson BC. Association of In Vivo [18F]AV-1451 Tau PET Imaging Results With Cortical Atrophy and Symptoms in Typical and Atypical Alzheimer Disease. JAMA Neurol. 2017;74(4):427-36.

789 9. Arriagada PV, Growdon JH, Hedley-Whyte ET, Hyman BT. Neurofibrillary tangles but not
790 senile plaques parallel duration and severity of Alzheimer's disease. Neurology. 1992;42(3 Pt
791 1):631-9.
792 10. Chen SD, Lu JY, Li HQ, Yang YX, Jiang JH, Cui M, Zuo CT, Tan L, Dong Q, Yu JT, Alzheimer's
793 Disease Neuroimaging I. Staging tau pathology with tau PET in Alzheimer's disease: a
794 longitudinal study. Transl Psychiatry. 2021;11(1):483.
795 11. Braak H, Thal DR, Ghebremedhin E, Del Tredici K. Stages of the pathologic process in
796 Alzheimer disease: age categories from 1 to 100 years. J Neuropathol Exp Neurol.
797 2011;70(11):960-9.
798 12. Braak H, Alafuzoff I, Arzberger T, Kretzschmar H, Del Tredici K. Staging of Alzheimer
799 disease-associated neurofibrillary pathology using paraffin sections and immunocytochemistry.
800 Acta Neuropathol. 2006;112(4):389-404.
801 13. Guo JL, Narasimhan S, Changolkar L, He Z, Stieber A, Zhang B, Gathagan RJ, Iba M,
802 McBride JD, Trojanowski JQ, Lee VM. Unique pathological tau conformers from Alzheimer's
803 brains transmit tau pathology in nontransgenic mice. J Exp Med. 2016;213(12):2635-54.
804 14. Roemer-Cassiano SN, Wagner F, Evangelista L, Rauchmann BS, Dehsarvi A, Steward A,
805 Dewenter A, Biel D, Zhu Z, Pescoller J, Gross M, Perneczky R, Malpetti M, Ewers M, Scholl M,
806 Dichgans M, Hoglinger GU, Brendel M, Jakel S, Franzmeier N. Amyloid-associated
807 hyperconnectivity drives tau spread across connected brain regions in Alzheimer's disease. Sci
808 Transl Med. 2025;17(782):eadp2564.
809 15. Tok S, Maurin H, Delay C, Crauwels D, Manyakov NV, Van Der Elst W, Moechars D,
810 Drinkenburg W. Pathological and neurophysiological outcomes of seeding human-derived tau
811 pathology in the APP-KI NL-G-F and NL-NL mouse models of Alzheimer's Disease. Acta
812 Neuropathol Commun. 2022;10(1):92.
813 16. He Z, Guo JL, McBride JD, Narasimhan S, Kim H, Changolkar L, Zhang B, Gathagan RJ, Yue
814 C, Dengler C, Stieber A, Nitla M, Coulter DA, Abel T, Brunden KR, Trojanowski JQ, Lee VM.
815 Amyloid-beta plaques enhance Alzheimer's brain tau-seeded pathologies by facilitating neuritic
816 plaque tau aggregation. Nat Med. 2018;24(1):29-38.
817 17. Wu JW, Hussaini SA, Bastille IM, Rodriguez GA, Mrejeru A, Rilett K, Sanders DW, Cook C,
818 Fu H, Boonen RA, Herman M, Nahmani E, Emrani S, Figueroa YH, Diamond MI, Clelland CL, Wray
819 S, Duff KE. Neuronal activity enhances tau propagation and tau pathology in vivo. Nat Neurosci.
820 2016;19(8):1085-92.
821 18. Vogel JW, Corriveau-Lecavalier N, Franzmeier N, Pereira JB, Brown JA, Maass A, Botha H,
822 Seeley WW, Bassett DS, Jones DT, Ewers M. Connectome-based modelling of
823 neurodegenerative diseases: towards precision medicine and mechanistic insight. Nat Rev
824 Neurosci. 2023;24(10):620-39.
825 19. Cornblath EJ, Li HL, Changolkar L, Zhang B, Brown HJ, Gathagan RJ, Olufemi MF,
826 Trojanowski JQ, Bassett DS, Lee VMY, Henderson MX. Computational modeling of tau pathology
827 spread reveals patterns of regional vulnerability and the impact of a genetic risk factor. Sci Adv.
828 2021;7(24).
829 20. Seemiller J, Bischof GN, Hoenig MC, Tahmasian M, van Eimeren T, Drzezga A, and the
830 Alzheimer's Disease Neuroimaging I. Indication of retrograde tau spreading along Braak stages
831 and functional connectivity pathways. Eur J Nucl Med Mol Imaging. 2021;48(7):2272-82.

832 21. Franzmeier N, Neitzel J, Rubinski A, Smith R, Strandberg O, Ossenkoppele R, Hansson O,
833 Ewers M, Alzheimer's Disease Neuroimaging I. Functional brain architecture is associated with
834 the rate of tau accumulation in Alzheimer's disease. Nat Commun. 2020;11(1):347.
835 22. Tok S, Ahnaou A, Drinkenburg W. Functional Neurophysiological Biomarkers of Early-
836 Stage Alzheimer's Disease: A Perspective of Network Hyperexcitability in Disease Progression. J
837 Alzheimers Dis. 2022;88(3):809-36.
838 23. Vossel KA, Tartaglia MC, Nygaard HB, Zeman AZ, Miller BL. Epileptic activity in
839 Alzheimer's disease: causes and clinical relevance. Lancet Neurol. 2017;16(4):311-22.
840 24. Gourmaud S, Stewart DA, Irwin DJ, Roberts N, Barbour AJ, Eberwine G, O'Brien WT,
841 Vassar R, Talos DM, Jensen FE. The role of mTORC1 activation in seizure-induced exacerbation
842 of Alzheimer's disease. Brain. 2022;145(1):324-39.
843 25. Horvath AA, Papp A, Zsuffa J, Szucs A, Luckl J, Radai F, Nagy F, Hidasi Z, Csukly G, Barcs
844 G, Kamondi A. Subclinical epileptiform activity accelerates the progression of Alzheimer's
845 disease: A long-term EEG study. Clin Neurophysiol. 2021;132(8):1982-9.
846 26. Baker J, Libretto T, Henley W, Zeman A. A Longitudinal Study of Epileptic Seizures in
847 Alzheimer's Disease. Front Neurol. 2019;10:1266.
848 27. Voglein J, Ricard I, Noachtar S, Kukull WA, Dieterich M, Levin J, Danek A. Seizures in
849 Alzheimer's disease are highly recurrent and associated with a poor disease course. J Neurol.
850 2020;267(10):2941-8.
851 28. Barbour AJ, Gourmaud S, Lancaster E, Li X, Stewart DA, Hoag KF, Irwin DJ, Talos DM,
852 Jensen FE. Seizures exacerbate excitatory: inhibitory imbalance in Alzheimer's disease and
853 5XFAD mice. Brain. 2024;147(6):2169-84.
854 29. Gourmaud S, Shou H, Irwin DJ, Sansalone K, Jacobs LM, Lucas TH, Marsh ED, Davis KA,
855 Jensen FE, Talos DM. Alzheimer-like amyloid and tau alterations associated with cognitive
856 deficit in temporal lobe epilepsy. Brain. 2020;143(1):191-209.
857 30. Siskova Z, Justus D, Kaneko H, Friedrichs D, Henneberg N, Beutel T, Pitsch J, Schoch S,
858 Becker A, von der Kammer H, Remy S. Dendritic structural degeneration is functionally linked to
859 cellular hyperexcitability in a mouse model of Alzheimer's disease. Neuron. 2014;84(5):1023-33.
860 31. Busche MA, Eichhoff G, Adelsberger H, Abramowski D, Wiederhold KH, Haass C,
861 Staufenbiel M, Konnerth A, Garaschuk O. Clusters of hyperactive neurons near amyloid plaques
862 in a mouse model of Alzheimer's disease. Science. 2008;321(5896):1686-9.
863 32. Zott B, Simon MM, Hong W, Unger F, Chen-Engerer HJ, Frosch MP, Sakmann B, Walsh
864 DM, Konnerth A. A vicious cycle of beta amyloid-dependent neuronal hyperactivation. Science.
865 2019;365(6453):559-65.
866 33. Zou Y, Wang C, Li H, Zhong M, Lin J, Hu Y, Chen Z, Gan CL. Epileptic seizures induced by
867 pentylenetetrazole kindling accelerate Alzheimer-like neuropathology in 5xFAD mice. Front
868 Pharmacol. 2024;15:1500105.
869 34. Allen WE, DeNardo LA, Chen MZ, Liu CD, Loh KM, Fenno LE, Ramakrishnan C, Deisseroth
870 K, Luo L. Thirst-associated preoptic neurons encode an aversive motivational drive. Science.
871 2017;357(6356):1149-55.
872 35. DeNardo LA, Liu CD, Allen WE, Adams EL, Friedmann D, Fu L, Guenthner CJ, Tessier-
873 Lavigne M, Luo L. Temporal evolution of cortical ensembles promoting remote memory
874 retrieval. Nat Neurosci. 2019;22(3):460-9.

875 36. Xing B, Barbour AJ, Vithayathil J, Li X, Dutko S, Fawcett-Patel J, Lancaster E, Talos DM,
876 Jensen FE. Reversible synaptic adaptations in a subpopulation of murine hippocampal neurons
877 following early-life seizures. J Clin Invest. 2024.
878 37. Naik AA, Sun H, Williams CL, Weller DS, Julius Zhu J, Kapur J. Mechanism of seizure-
879 induced retrograde amnesia. Prog Neurobiol. 2021;200:101984.
880 38. Naik AA, Brodovskaya A, Subedi S, Akram A, Kapur J. Extrahippocampal seizure and
881 memory circuits overlap. eNeuro. 2022;9(4).
882 39. Oakley H, Cole SL, Logan S, Maus E, Shao P, Craft J, Guillozet-Bongaarts A, Ohno M,
883 Disterhoft J, Van Eldik L, Berry R, Vassar R. Intraneuronal beta-amyloid aggregates,
884 neurodegeneration, and neuron loss in transgenic mice with five familial Alzheimer's disease
885 mutations: potential factors in amyloid plaque formation. J Neurosci. 2006;26(40):10129-40.
886 40. Dimmock S, Exley BMS, Moore G, Menage L, Delogu A, Schultz SR, Warburton EC,
887 Houghton C, O'Donnell C. Hierarchical Bayesian modeling of multi-region brain cell count data.
888 eLife. 2024;13(RP102391).
889 41. Brevard ME, Kulkarni P, King JA, Ferris CF. Imaging the neural substrates involved in the
890 genesis of pentylenetetrazol-induced seizures. Epilepsia. 2006;47(4):745-54.
891 42. Coulter DA, Huguenard JR, Prince DA. Differential effects of petit mal anticonvulsants
892 and convulsants on thalamic neurones: calcium current reduction. Br J Pharmacol.
893 1990;100(4):800-6.
894 43. Henderson MX, Cornblath EJ, Darwich A, Zhang B, Brown H, Gathagan RJ, Sandler RM,
895 Bassett DS, Trojanowski JQ, Lee VMY. Spread of alpha-synuclein pathology through the brain
896 connectome is modulated by selective vulnerability and predicted by network analysis. Nat
897 Neurosci. 2019;22(8):1248-57.
898 44. Oh SW, Harris JA, Ng L, Winslow B, Cain N, Mihalas S, Wang Q, Lau C, Kuan L, Henry AM,
899 Mortrud MT, Ouellette B, Nguyen TN, Sorensen SA, Slaughterbeck CR, Wakeman W, Li Y, Feng
900 D, Ho A, Nicholas E, Hirokawa KE, Bohn P, Joines KM, Peng H, Hawrylycz MJ, Phillips JW,
901 Hohmann JG, Wohnoutka P, Gerfen CR, Koch C, Bernard A, Dang C, Jones AR, Zeng H. A
902 mesoscale connectome of the mouse brain. Nature. 2014;508(7495):207-14.
903 45. Iba M, McBride JD, Guo JL, Zhang B, Trojanowski JQ, Lee VM. Tau pathology spread in
904 PS19 tau transgenic mice following locus coeruleus (LC) injections of synthetic tau fibrils is
905 determined by the LC's afferent and efferent connections. Acta Neuropathol. 2015;130(3):349-
906 62.
907 46. Ahnaou A, Walsh C, Manyakov NV, Youssef SA, Drinkenburg WH. Early
908 Electrophysiological Disintegration of Hippocampal Neural Networks in a Novel Locus Coeruleus
909 Tau-Seeding Mouse Model of Alzheimer's Disease. Neural Plast. 2019;2019:6981268.
910 47. Korzhova V, Marinkovic P, Njavro JR, Goltstein PM, Sun F, Tahirovic S, Herms J, Liebscher
911 S. Long-term dynamics of aberrant neuronal activity in awake Alzheimer's disease transgenic
912 mice. Commun Biol. 2021;4(1):1368.
913 48. Shokouhi S, Taylor WD, Albert K, Kang H, Newhouse PA, Alzheimer's Disease
914 Neuroimaging I. In vivo network models identify sex differences in the spread of tau pathology
915 across the brain. Alzheimers Dement (Amst). 2020;12(1):e12016.
916 49. Wang YT, Therriault J, Servaes S, Tissot C, Rahmouni N, Macedo AC, Fernandez-Arias J,
917 Mathotaarachchi SS, Benedet AL, Stevenson J, Ashton NJ, Lussier FZ, Pascoal TA, Zetterberg H,
918 Rajah MN, Blennow K, Gauthier S, Rosa-Neto P, Alzheimer's Disease Neuroimaging I. Sex-

919 specific modulation of amyloid-beta on tau phosphorylation underlies faster tangle
920 accumulation in females. Brain. 2024;147(4):1497-510.
921 50. Deleyto-Seldas N, Efeyan A. The mTOR-Autophagy Axis and the Control of Metabolism.
922 Front Cell Dev Biol. 2021;9:655731.
923 51. Lin H, Leng X, Qin C, Wang W, Zhang C, Qiu S. Altered White Matter Structural Network
924 in Frontal and Temporal Lobe Epilepsy: A Graph-Theoretical Study. Front Neurol. 2020;11:561.
925 52. Kreilkamp BAK, McKavanagh A, Alonazi B, Bryant L, Das K, Wieshmann UC, Marson AG,
926 Taylor PN, Keller SS. Altered structural connectome in non-lesional newly diagnosed focal
927 epilepsy: Relation to pharmacoresistance. Neuroimage Clin. 2021;29:102564.
928 53. Zhang Z, Liao W, Chen H, Mantini D, Ding JR, Xu Q, Wang Z, Yuan C, Chen G, Jiao Q, Lu G.
929 Altered functional-structural coupling of large-scale brain networks in idiopathic generalized
930 epilepsy. Brain. 2011;134(Pt 10):2912-28.
931 54. Liang Y, Chen C, Li F, Yao D, Xu P, Yu L. Altered Functional Connectivity after Epileptic
932 Seizure Revealed by Scalp EEG. Neural Plast. 2020;2020:8851415.
933 55. Tabuas-Pereira M, Duraes J, Lopes J, Sales F, Bento C, Duro D, Santiago B, Almeida MR,
934 Leitao MJ, Baldeiras I, Santana I. Increased CSF tau is associated with a higher risk of seizures in
935 patients with Alzheimer's disease. Epilepsy Behav. 2019;98(Pt A):207-9.
936 56. Lam AD, Thibault EG, Mayblyum DV, Hsieh S, Pellerin KR, Sternberg EJ, Viswanathan A,
937 Buss S, Sarkis RA, Jacobs HIL, Johnson KA, Sperling RA. Association of Seizure Foci and Location
938 of Tau and Amyloid Deposition and Brain Atrophy in Patients With Alzheimer Disease and
939 Seizures. Neurology. 2024;103(9):e209920.
940 57. Bakker A, Krauss GL, Albert MS, Speck CL, Jones LR, Stark CE, Yassa MA, Bassett SS,
941 Shelton AL, Gallagher M. Reduction of hippocampal hyperactivity improves cognition in
942 amnestic mild cognitive impairment. Neuron. 2012;74(3):467-74.
943 58. Vossel K, Ranasinghe KG, Beagle AJ, La A, Ah Pook K, Castro M, Mizuiri D, Honma SM,
944 Venkateswaran N, Koestler M, Zhang W, Mucke L, Howell MJ, Possin KL, Kramer JH, Boxer AL,
945 Miller BL, Nagarajan SS, Kirsch HE. Effect of Levetiracetam on Cognition in Patients With
946 Alzheimer Disease With and Without Epileptiform Activity: A Randomized Clinical Trial. JAMA
947 Neurol. 2021;78(11):1345-54.
948 59. Henderson MX, D'weerd D, Kurgat K. Mouse Brain Heatmap - Whole brain data
949 compilation and quality control. protocolsio. 2024.
950 60. Fox J, editor Bootstrapping Regression Models Appendix to An R and S-PLUS Companion
951 to Applied Regression2002.
952

953 # Acknowledgements

954 These studies were funded by the National Institutes of Health (NIH) National Institute on Aging
955 (NIA) T32AG000255 (AJB) and R01AG077092 (FEJ and DMT), the Alzheimer's Association
956 AARF-22-972333 (AJB), the NIH National Institute of Neurological Disorders and Stroke
957 (NINDS): R01NS101156 (DMT) and R37NS115439 (FEJ). Postmortem tissue and clinical data

958 from control and Alzheimer's disease was collected with funding from the NIH NIA:
959 P30AG072979, P01AG084497, and R01AG054519.
960 We would like to thank The Neurobehavior Testing Core at UPenn/ITMAT and IDDRC at
961 CHOP/Penn U54 HD086984 for assistance with the behavior procedures. We also thank the
962 Center for Neurodegenerative Disease Research (CNDR) at the University of Pennsylvania for
963 providing human Alzheimer's disease and control samples and relevant clinical and
964 neuropathology information. We also would like to thank Lakshmi Changolkar for her work to
965 isolate the AD-tau used in these studies. Schematics in Figures 1 and 8 were created in
966 BioRender.

967 # Author Contributions

968 AJB, VMYL, DMT, and FEJ conceptualized the studies in the manuscript. AJB, KH, AC, XL, SZ,
969 and CH performed experiments, analyzed data, and prepared figures. EJC, AL, and KAD
970 performed computational analyses and prepared figures. EBL performed pathological ratings for
971 human postmortem analysis and assisted with clinical data reports. AJB, DMT, and FEJ wrote
972 the manuscript. All authors read and approved the manuscript.
973
974
975
976

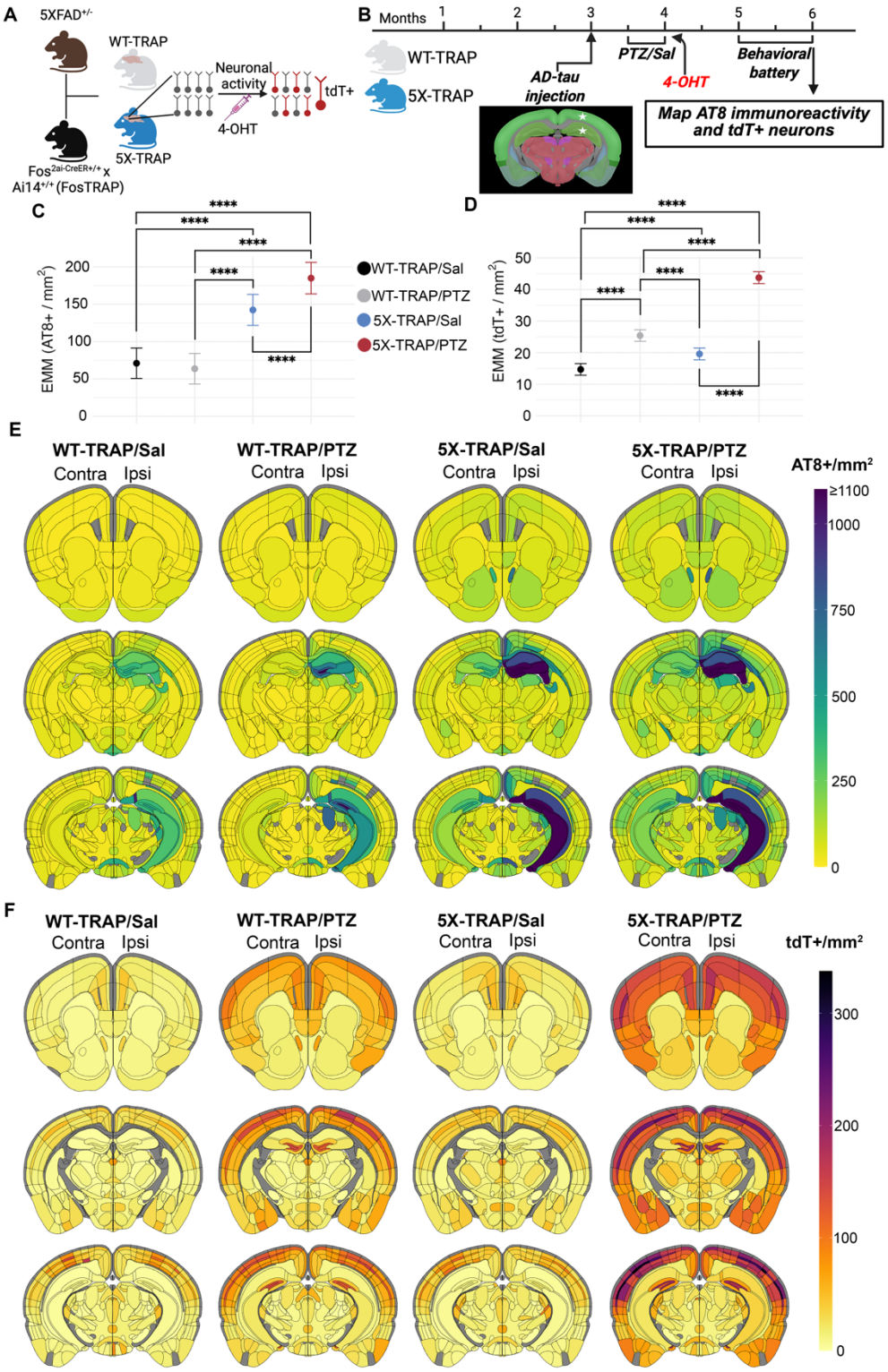

977

978 **Figure 1. Brain mapping reveals increased tau spread in 5X-TRAP mice that is**

979 **exacerbated by seizure induction and increased tdT+ labeling in PTZ and saline treated**

980 **5X-TRAP mice.** (**A**) Schematic for the generation of, and activity-dependent labelling in WT-
981 TRAP and 5X-TRAP mice. (**B**) Experimental timeline: WT-TRAP and 5X-TRAP mice underwent
982 AD-tau seeding at three months of age in the right dorsal hippocampus and overlying cortex
983 (posterior parietal association area) (star=injection sites), PTZ seizure kindling (or control, Sal
984 injection) at 3.5-4 months of age, and behavioral battery at 5-6 months of age prior to brain
985 collection for mapping studies. We performed linear mixed models with (**C**) AT8+/mm^2 and (**D**)
986 tdT+ cells/mm^2 as dependent variables, genotype and treatment as fixed effects, and brain
987 region/animal as random effects. We found significant interactions between 5XFAD genotype
988 and PTZ treatment to increase brain-wide AT8+ levels (β=49.97, SE=9.07, t (15938)=5.51,
989 $p<0.0001$) and tdT+ counts (β=13.42, SE=1.05, t (15938)=12.81, $p<0.0001$). (**C**) Pairwise
990 comparisons were conducted using estimated marginal means (EMM) which revealed a
991 significant increase in brain-wide AT8+ levels in 5X-TRAP groups compared to WT-TRAP and
992 in PTZ kindled 5X-TRAP compared to Sal treated 5X-TRAP. Points represent EMM and bars
993 represent 95% confidence intervals. Tukey's post hoc: ****=$p<0.0001$. (**D**) Pairwise comparisons
994 of EMM revealed a significant increase in tdT+ counts in Sal and PTZ treated 5X-TRAP
995 compared to Sal and PTZ Treated WT-TRAP, respectively, and in PTZ treated 5X-TRAP and
996 WT-TRAP compared to Sal treated 5X-TRAP and WT-TRAP. Three coronal sections from the
997 Allen Brain Atlas for each experimental group displaying heatmaps for mean detected (**E**) AT8+
998 immunoreactive aggregates/mm^2 and (**F**) tdT+ counts/mm^2. Representative images of AT8 and
999 tdT fluorescence can be found in Fig S3 and the mean, SEM, sample size, and statistical results
1000 for region/subregion AT8+ levels and tdT+ counts can be found in Tables S1, S2.
1001
1002

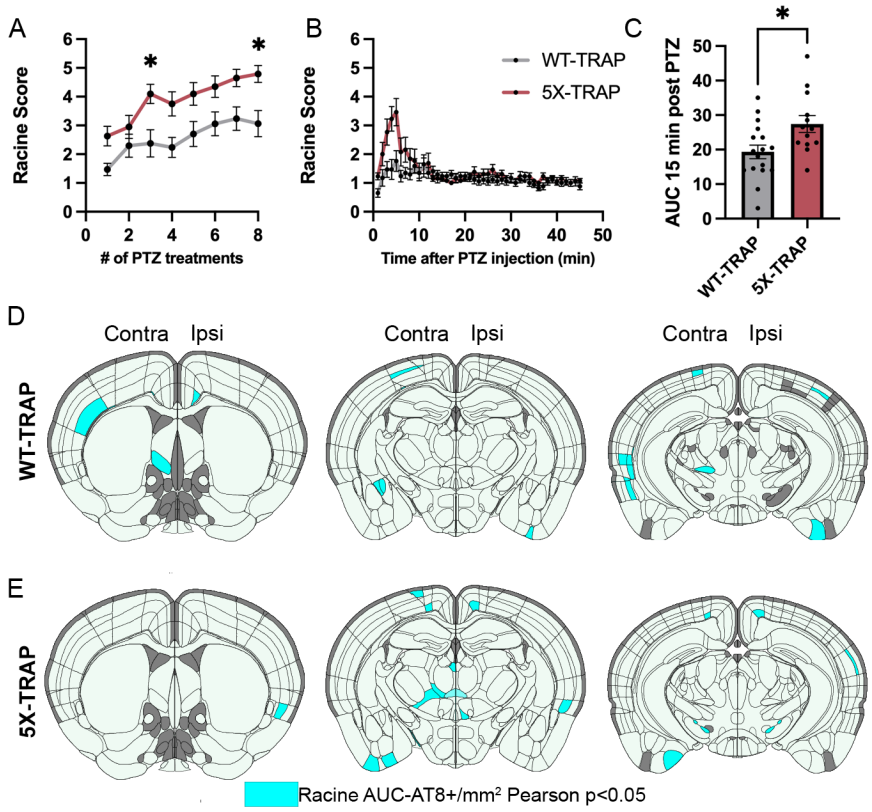

Figure 2. Seizure severity is increased in 5X-TRAP mice and is correlated with tau spread and activity dependent labeling. (**A**) Repeated measure (RM) two-way ANOVA with number of treatments (RM) and genotype as independent variables was performed for maximal daily seizure severity (Racine score). WT-TRAP and 5X-TRAP mice showed increasing seizure severity over the course of kindling (treatment #: $F_{4.95, 171.6}$=15.27, p<0.0001), with 5X-TRAP mice reaching higher maximal Racine score in the 45 minutes following PTZ administration compared to WT-TRAP mice (genotype: $F_{1, 35}$=9.71, p<0.01). Sidak's post hoc: *=p<0.05, n= 17 (WT-TRAP)-21 (5X-TRAP). (**B**) Maximal Racine score per minute was recorded during the final PTZ administration. (**C**) 5X-TRAP mice have significantly increased area under the curve (AUC) during the first 15 minutes of the final PTZ administration. Two-tailed t-test: *=p<0.05. Brain atlas heatmaps highlight brain regions with significant positive Pearson correlations between AT8+/mm^2 and seizure severity (Racine AUC) in PTZ kindled (**D**) 5X-TRAP mice and (**E**) WT-

TRAP mice. No significant negative correlations were found. Scatter plots for these correlations can be found in Figure S5, S6. Histograms display group mean ± SEM.

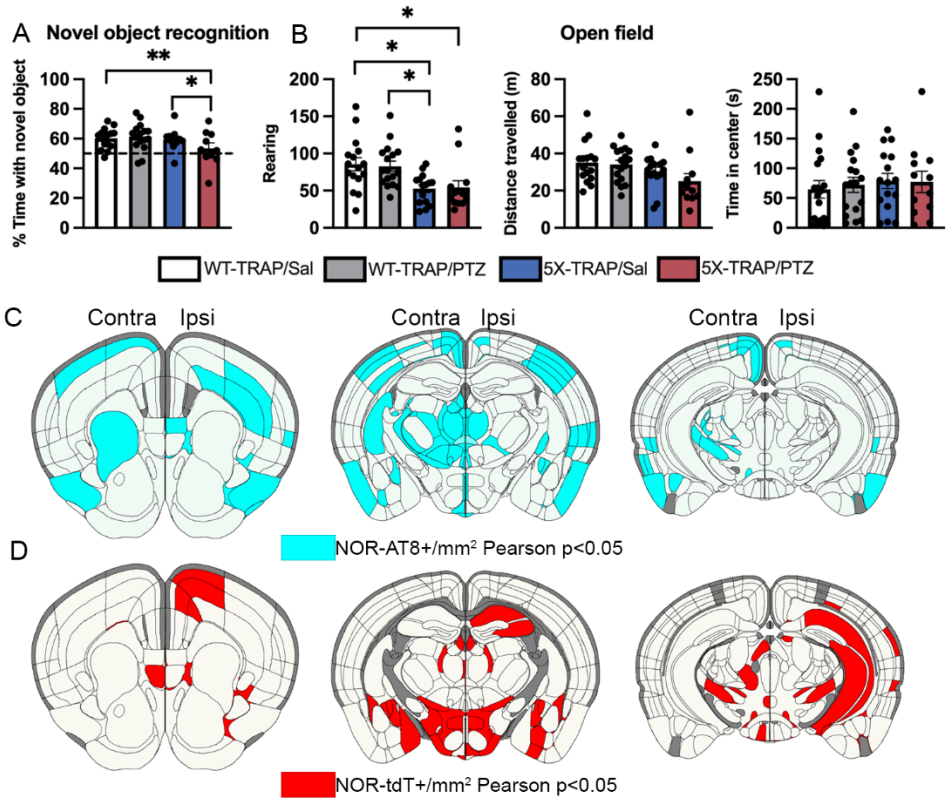

Figure 3. Memory deficits in PTZ kindled 5X-TRAP mice are correlated with tau spread and network hyperactivity. Two-way ANOVA with genotype (WT-TRAP vs 5X-TRAP) and kindling (Sal vs PTZ) were performed for behavioral tests (**A**, **B**). (**A**) PTZ-kindled 5X-TRAP mice had significantly decreased % time spent with novel object compared to saline treated 5X-TRAP and WT-TRAP mice (interaction: $F_{1,49}$=4.45, p<0.05). (**B**) 5X-TRAP mice showed reduced rearing behavior (left; genotype effect: $F_{1,58}$=17.21, p<0.0001) and total distance travelled (center; genotype effect: $F_{1,56}$=6.01, p<0.05) without change in time spent in center (right). *, **=Sidak's post hoc p<0.05, 0.01; n=10-16/group. Brain atlas heatmaps highlight brain regions with significant negative Pearson correlations between % time spent with novel object in the NOR task and (**C**) AT8+/mm^2 and (**D**) tdT+ aggregates/mm^2 in PTZ kindled 5X-TRAP mice. No significant positive correlations were found. Scatter plots for these correlations can be found in Figures S10, S11. Histograms display group mean ± SEM.

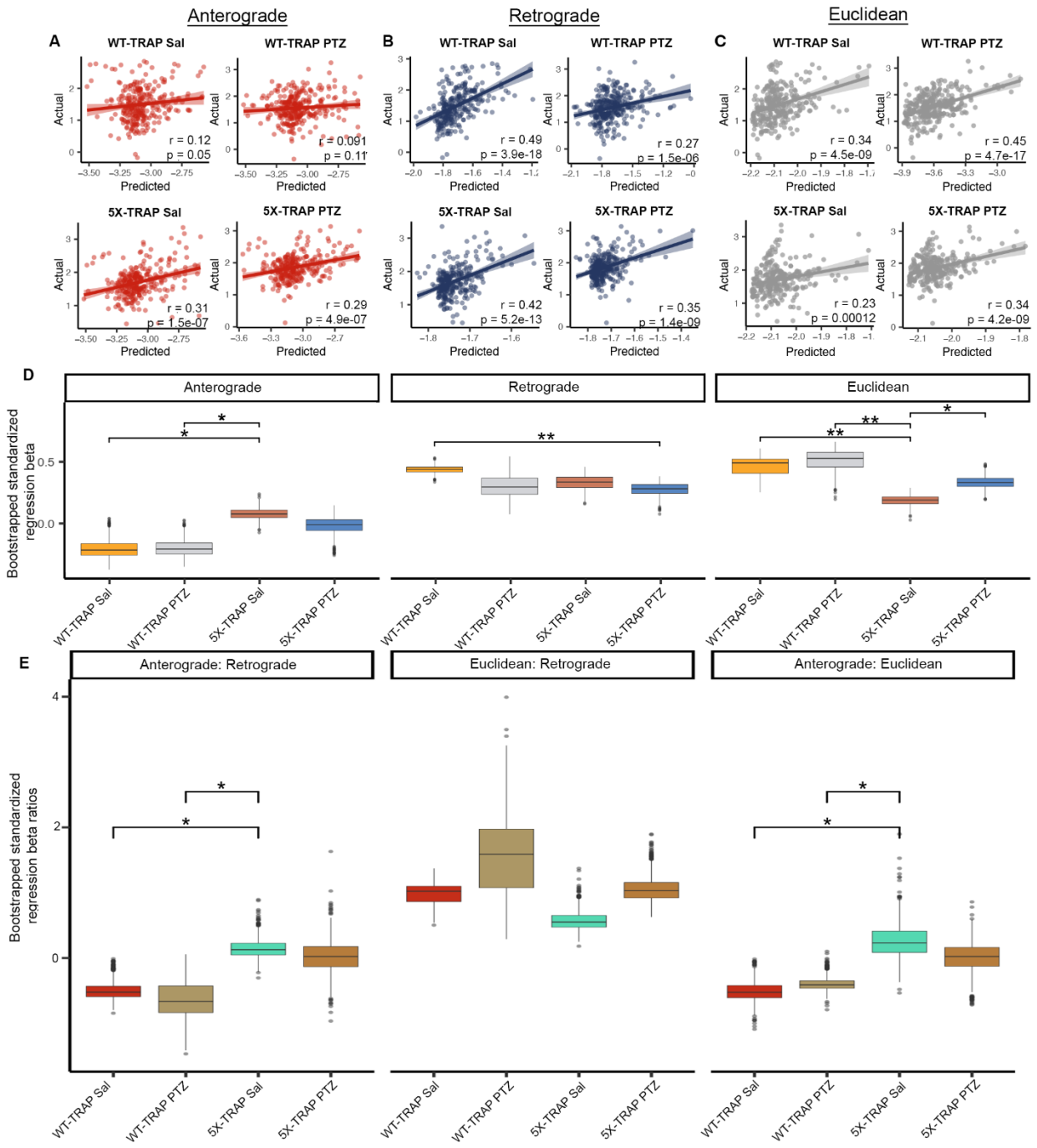

Figure 4. Computational modeling reveals an increased impact of anterograde tau spread in 5X-TRAP mice. Predictions of tau spread based on (**A**) anterograde, (**B**) retrograde, and (**C**) Euclidean models of spread plotted against our measured levels for each experimental group. Solid lines represent best fit and shaded regions are the 95% confidence interval. (**D**) For the Bidirectional Euclidean + tdT spread model architecture, we performed a bootstrap comparison

of mean standardized regression beta weights between groups and adjusted for multiple comparisons. (**E**) For the Bidirectional Euclidean spread model architecture, we performed a bootstrap comparison of mean ratio of standardized anterograde: retrograde, Euclidean: retrograde, and anterograde: Euclidean regression beta weights between groups and adjusted for multiple comparisons. p-values were adjusted for multiple comparisons in each panel using FDR correction: *$p<0.05$, **$p<0.01$. Box plots boxes display the median, 25th and 75th percentiles, and whiskers extend to the data point that is at most 1.5 x interquartile range, and data beyond this point are plotted individually.

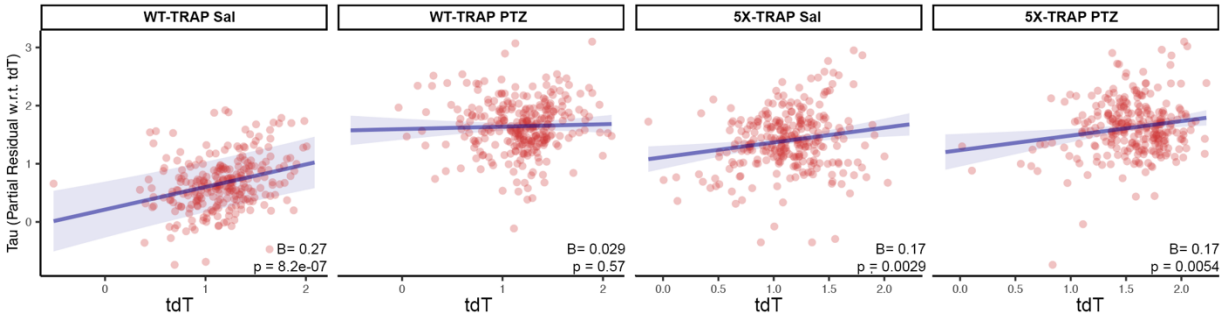

Figure 5. Regional tdT+ levels are predictive of tau spread. We fit a linear regression model separately for WT-TRAP and 5X-TRAP mice to estimate regional tau pathology using anterograde spread, retrograde spread, Euclidean distance-based spread, tdT+ cell density, and interactions between PTZ treatment and tdT positive cell density as predictor variables. In the plots above, we show partial residual plots of tau pathology (y-axis) versus tdT cell density (x-axis) for each level of the interaction with PTZ treatment (i.e. PTZ and Saline) while controlling for estimated anterograde, retrograde, and Euclidean distance-based spread. Individual points correspond to anatomical regions with available tdT+ cell density (n = 6-15 mice/group/brain region; 261-288 brain regions/group). tdT+ levels were predictive of tau spread in all groups except PTZ treated WT-TRAP mice. p-values test the significance of simple slopes of tdT as a predictor of AT8+ levels for each group.

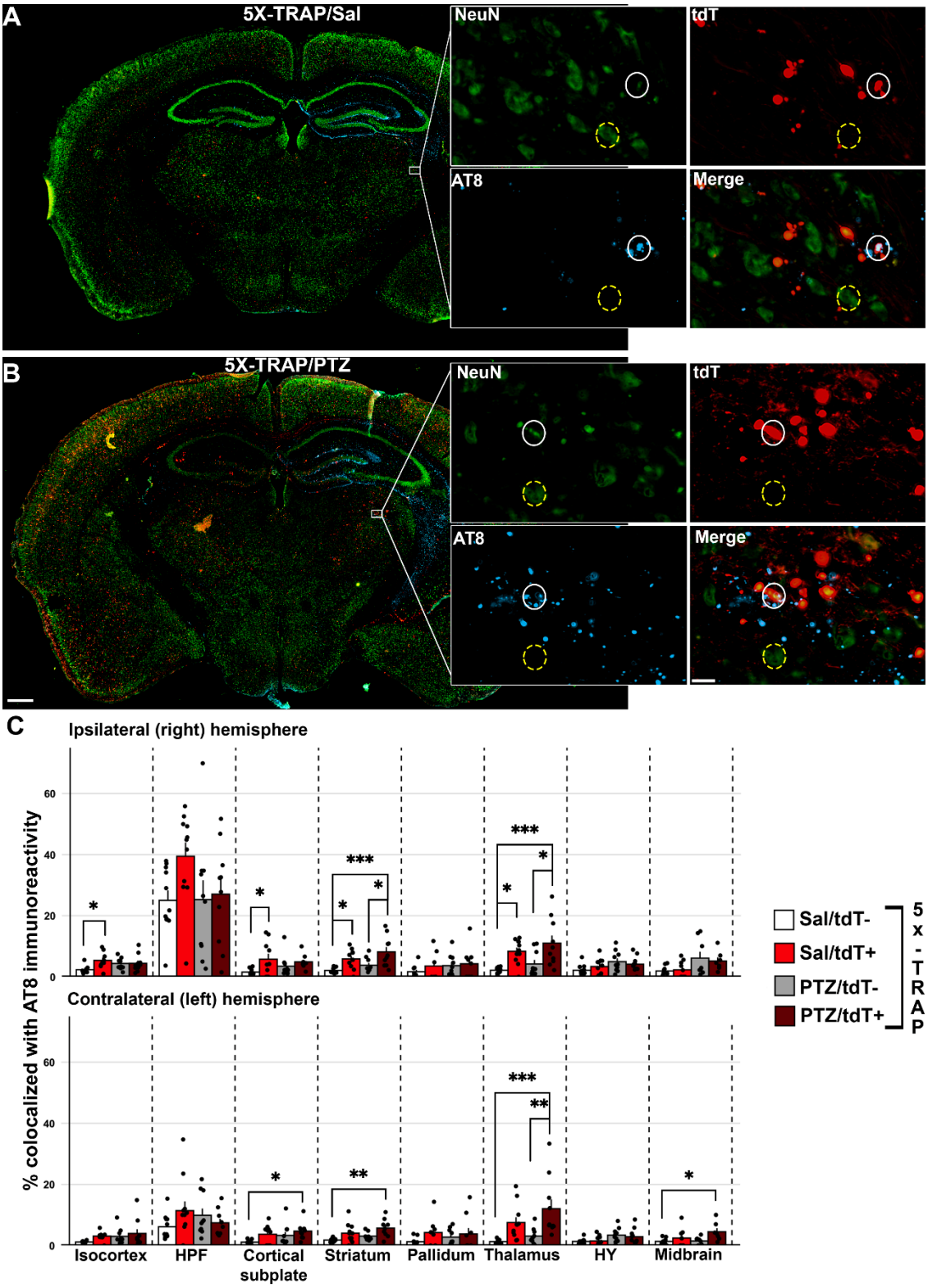

Figure 6. tdT+ neurons are more likely to colocalize with tau pathology in both saline and PTZ treated 5X-TRAP mice. Representative slide scanned coronal sections from (**A**) saline

1089 and (**B**) PTZ treated 5X-TRAP mice. Inset displays thalamic tdT+ (white circles) and tdT-
1090 (NeuN+) (yellow dashed circles) neurons colocalization with AT8+ immunoreactive aggregates.
1091 Scale bars = 500 μm, 20 μm (inset). (**C**) tdT+, tdT-, and colocalized AT8+ cells were mapped to
1092 the Allen Brain Atlas and % of detected tdT+/tdT- cells were quantified in 9 major brain
1093 structures, bilaterally. A two-way ANOVA was performed with treatment (Sal vs PTZ) and cell
1094 type (tdT- vs tdT+) as independent variables for each brain region. There was a significant
1095 increase in percentage of tdT+ neurons colocalized with AT8 than surrounding tdT- in Sal
1096 treated 5X-TRAP mice in the ipsilateral thalamus (cell type: $F_{1,38}$=19.17, $p<0.0001$), striatum
1097 (treatment: $F_{1,38}$=4.39, $p<0.05$; cell type: $F_{1,38}$=17.62, $p<0.001$), and isocortex ($F_{1,34}$=4.12,
1098 $p<0.05$). There was a significant increase in % tdT+ neurons colocalized with AT8+ than
1099 surrounding tdT- cells in PTZ treated mice in the ipsilateral thalamus and striatum and
1100 contralateral thalamus (cell type: $F_{1,38}$=18.60, $p<0.001$). Tukey's post hoc: *$p<0.05$, **$p<0.01$,
1101 ***$p<0.001$; n=7-11/group/brain region. Histograms display group mean ± SEM.
1102
1103
1104
1105
1106
1107
1108
1109
1110
1111
1112
1113
1114
1115
1116
1117
1118

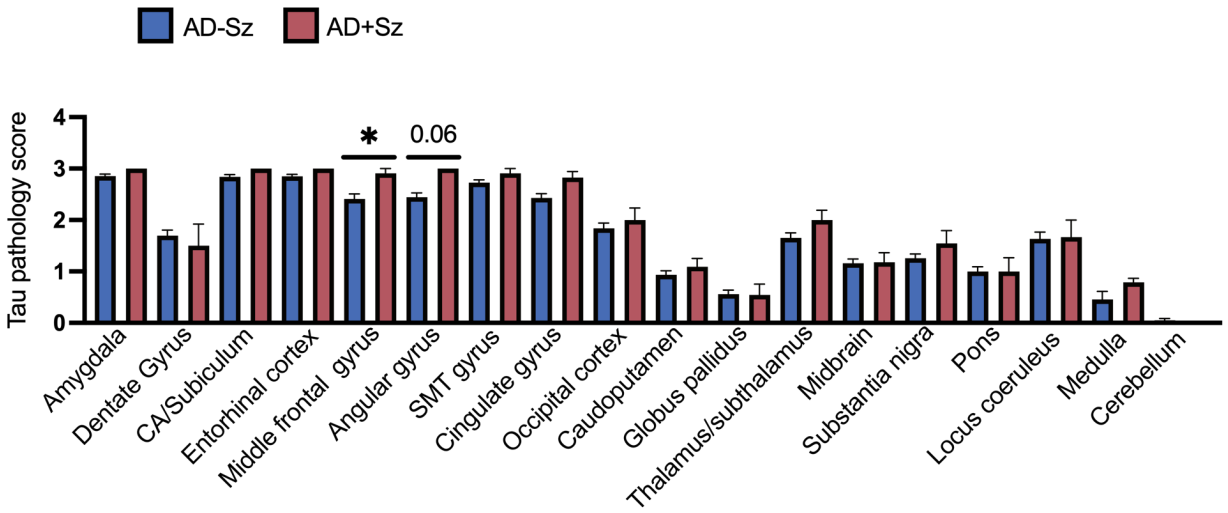

Figure 7. Worsened tau pathology in AD patients with a history of seizures. Tau pathology severity ratings from postmortem analysis of AD-Sz and AD+Sz were compared by two-tailed Mann-Whitney test. AD+Sz had significantly increased tau rating compared to AD-Sz in the middle frontal gyrus and a strong trend in the angular gyrus. *$p<0.05$, AD-Sz n= 74-95/brain region, AD+Sz n=8-11/brain region. SMT gyrus= superior/middle temporal gyrus. Histograms display group mean ± SEM.

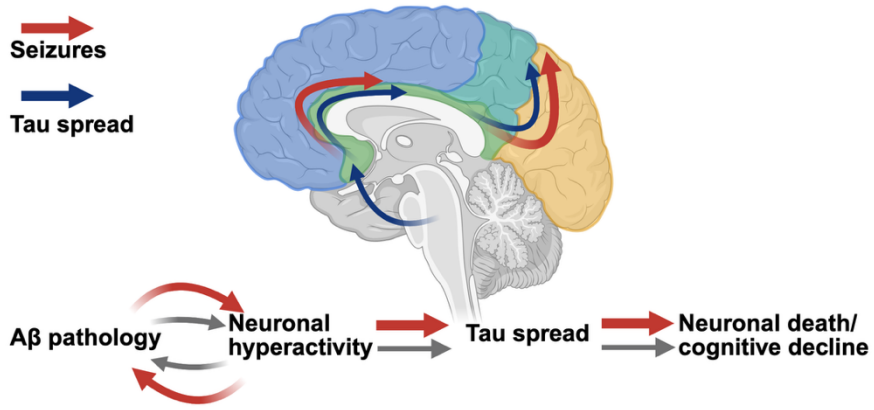

Figure 8. Schematic of proposed model for AD progression.